390
6-9-81

(2)

Dr. 2720

DOE/JPL/954331-81/13

SILICON MATERIALS TASK OF THE LOW-COST SOLAR ARRAY PROJECT (PHASE IV)

MASTER

Effects of Impurities and Processing on Silicon Solar Cells

Twenty-First Quarterly Report, October—December 1980

By
R. H. Hopkins
M. H. Hanes
J. R. Davis
A. Rohatgi
P. Rai-Choudhury
H. C. Mollenkopf

D124-243
NTIS-25

January 30, 1981

Work Performed Under Contract No. NAS-7-100-954331

Westinghouse R&D Center
Pittsburgh, Pennsylvania

U.S. Department of Energy

Solar Energy

DISCLAIMER

This report was prepared as an account of work sponsored by an agency of the United States Government. Neither the United States Government nor any agency Thereof, nor any of their employees, makes any warranty, express or implied, or assumes any legal liability or responsibility for the accuracy, completeness, or usefulness of any information, apparatus, product, or process disclosed, or represents that its use would not infringe privately owned rights. Reference herein to any specific commercial product, process, or service by trade name, trademark, manufacturer, or otherwise does not necessarily constitute or imply its endorsement, recommendation, or favoring by the United States Government or any agency thereof. The views and opinions of authors expressed herein do not necessarily state or reflect those of the United States Government or any agency thereof.

DISCLAIMER

Portions of this document may be illegible in electronic image products. Images are produced from the best available original document.

DISCLAIMER

"This book was prepared as an account of work sponsored by an agency of the United States Government. Neither the United States Government nor any agency thereof, nor any of their employees, makes any warranty, express or implied, or assumes any legal liability or responsibility for the accuracy, completeness, or usefulness of any information, apparatus, product, or process disclosed, or represents that its use would not infringe privately owned rights. Reference herein to any specific commercial product, process, or service by trade name, trademark, manufacturer, or otherwise, does not necessarily constitute or imply its endorsement, recommendation, or favoring by the United States Government or any agency thereof. The views and opinions of authors expressed herein do not necessarily state or reflect those of the United States Government or any agency thereof."

This report has been reproduced directly from the best available copy.

Available from the National Technical Information Service, U. S. Department of Commerce, Springfield, Virginia 22161.

Price: Printed Copy A04
Microfiche A01

DOE/JPL/954331-81/13
Distribution Category UC-63b

SILICON MATERIALS TASK OF THE LOW-COST SOLAR ARRAY PROJECT (PHASE IV)

Effects of Impurities and Processing on Silicon Solar Cells

Twenty-First Quarterly Report

January 30, 1981

October 1980-December 1980

R. H. Hopkins, M. H. Hanes, J. R. Davis, A. Rohatgi,
and P. Rai-Choudhury
Westinghouse Research and Development Center
and
H. C. Mollenkopf
Hemlock Semiconductor Corporation

TABLE OF CONTENTS

LIST OF TABLES

LIST OF FIGURES

LIST OF FIGURES (Cont.)

1. SUMMARY

The overall objective of this program is to define the effects of impurities, various thermochemical processes, and any impurity-process interactions upon the performance of terrestrial solar cells. The results of the study form a basis for silicon producers, wafer manufacturers, and cell fabricators to develop appropriate cost-benefit relationships for the use of less pure, less costly solar grade silicon.

Cr is highly mobile in silicon even at temperatures as low as 600°C. Contrasting with earlier data for Mo, Ti, and V, Cr concentrations vary from place to place in polycrystalline silicon wafers and the electrically-active Cr concentration in the polysilicon is more than an order of magnitude smaller than would be projected from single crystal impurity data. We hypothesize that Cr diffuses during ingot cooldown after growth, preferentially segregates to grain boundaries and becomes electrically deactivated.

Both Al and Au introduce deep levels when grown into silicon crystals. Al produces two levels, E_V+0.44eV and E_V+0.49eV, while Au gives rise to four levels, E_V+0.22eV, E_V+0.34eV, E_V+0.47eV, E_V+0.53eV. This latter result contrasts with the two Au levels usually observed following diffusion. Both the red response and cell performance of Al and Au-doped solar cells are degraded by deep level formation.

Accelerated aging data from Ni-contaminated silicon imply that no significant impurity-induced cell performance reduction should be expected over a twenty-year device lifetime.

Combined electrical bias and thermal stressing of silicon solar cells containing Nb, Fe, Cu, Ti, Cr, and Ag, respectively produces no performance loss after 100 hour exposures up to 225°C.

Ti and V, but not Mo, can be gettered from polycrystalline silicon by $POCl_3$ or HCl at temperatures of 1000°C and 1100°C.

2. INTRODUCTION

This is the twenty-first quarterly report describing activities conducted under JPL Contract 954331, and is the fourth report of the Phase IV studies.

In Phase III, "An Investigation of the Effects of Impurities and Processing on Silicon Solar Cells," the effects of thermal processes, impurities, and impurity-process interactions were determined and documented. The development of this data base led to a more precise definition of what constitutes an acceptable "Solar Grade" Silicon. In addition, it provided silicon manufacturers with a rationale for selection of construction materials; it has helped ingot, sheet, or ribbon manufacturers to specify the purity of silicon feedstocks; and it has enabled cell manufacturers to define acceptable wafer purities for cell fabrication and to choose processes which minimize adverse impurity effects. In short, the impurity effect data provide a basis for cost-benefit analysis to producers and users of Solar Grade Silicon.

In Phase IV of this program, the approaches and techniques developed in Phase III are being extended to several new areas, as well as to developing an improved data base for aging effects and certain process-related phenomena. The Phase IV tasks include (1) evaluation, by previously developed process techniques, of the properties of silicon produced by experimental low cost processes; (2) extending threshold impurity concentration data to high efficiency cells; (3) measuring the effects of interaction between impurities and grain boundaries in polycrystalline solar cells; (4) evaluating the long term effects of impurities in solar cells; and (5) examining the effects of processes such as ion implantation on contaminated solar cells.

During this quarter we have continued studies of polycrystalline solar cells, accelerated aging of impurity behavior, thermochemical processing and modeling of impurity effects in high efficiency devices. The results of that effort are described in the following sections.

3. TECHNICAL PROGRESS

3.1 Crystal Growth and Analysis

3.1.1 Ingot Preparation

During this quarter we have grown ingots with the intentionally-added impurities Au, Al and Mn respectively. The Au and Al-doped ingots were monocrystalline, while the Mn doped ingot was polycrystalline. Subsequently a second Mn ingot was grown (W231) using half the initial Mn concentration to help suppress excessive metal-rich inclusion formation and crystal structure breakdown.

Of the four p-type silicon ingots pulled for solar cell characterization, the Al-doped ingot contained only Al as the electrically active dopant and had a resistivity of 1.5 ohm-cm. The remaining ingots contained the usual intentionally added boron to yield resistivities near 4 ohm-cm. Each ingot's intentionally added metal impurity dopant, associated crystalline structure and task are indicated in Table 1. All ingots were prepared by the Czochralski crystal growth method with details of the crystal growth equipment and conditions found in earlier reports.[1,2]

3.1.2 Ingot Evaluation

Detailed ingot impurity data are indicated in Table 2 with the listing of ingot identification, intentionally added target impurity concentration, ingot impurity concentration based on melt analysis by atomic absorption (calculated concentration), and ingot seed impurity concentration measured by spark source mass spectrometry.[2,3]

Spark source mass spectrometer analyses of the first generation Au-doped ingot seed samples yielded an impurity concentration $<5\times10^{14}$ atoms/cm^3 (below sensitivity of mass spectrometer). However, spark source analyses of ingot tang samples produced a value of 5.5×10^{14} atoms/cm^3. The Au^{++}

TABLE 1 INGOT IMPURITY, STRUCTURE AND TASK

IMPURITY	STRUCTURE	TASK
Au	Single	Thermochemical Processing
Al	Single	Thermochemical Processing
Mn*	Polycrystalline	Polycrystalline

*Two ingot growths with the latter having reduced impurity concentration to suppress metal-rich inclusions.

TABLE 2 INGOT IMPURITY CONCENTRATION

Ingot Identification	Target Concentration $\times 10^{15}$ atoms/cm^3	Calculated Concentration $\times 10^{15}$ atoms/cm^3	Mass Sepc. Analysis $\times 10^{15}$ atoms/cm^3
W-198-00-000	None	N/A	None
W-199-00-000	None	N/A	None
W-200-V-004-Poly	0.4	0.38	18.5*
W-201-Mo-007-Poly	0.005	0.003	77*
W-202-Ti-013-Poly	0.02	0.018	0.25
W-203-V-005-Poly	0.04	0.053	0.15
W-204-Cr-008-Poly	1.0	0.82	1322*
W-205-Fe-009-Poly	0.5	0.61	1.5
W-206-V-006	0.02	0.026	0.15
W-207-Mo-008	0.002	0.002	0.5
W-208-Cr-009	0.2	0.19	0.6
W-209-Ti-014	0.02	0.024	0.25
W-210-Ti-015	0.08	0.10	0.25
W-211-Cu-007	1.0	1.0	2.6
W-212-Cu-008	10	12.5	27
W-213-Pb-001	Max. Conc.	Non Detectable	0.10+
W-214-V-007-Poly	0.20	0.30	0.55**
W-215-Mo-009-Poly	0.0025	0.002	0.5**
W-216-Cr-010-Poly	0.80	0.64	2.2**
W-217-Ta-005	0.00015	0.0003	0.5
W-218-Ta-006	0.000065	0.0001	0.5
W-219-V-008	0.007	0.009	0.15

TABLE 2 INGOT IMPURITY CONCENTRATION (continued)

Ingot Identification	Target Concentration x10^{15}atoms/cm^3	Calculated Concentration x10^{15}atoms/cm^3	Mass Spec. Analysis x10^{15}atoms/cm^3
W-220-W-005	0.0008	0.0007	0.15
W-221-Ni-005	10	8.2	1.5
W-222-Ag-002	4.5	3.2	6.0
W-223-Ni-006	1.0	1.1	1.5
W-224-HSC/DCS-57	NA^{++}	None	0.2^{+++}
W-225-Mn-00	1.0	1.5	5.5
W-226-Mn-010	4.0	***	***
W-227-Cr-011-Poly	0.4	0.43	2.2
W-228-Gd-001	0.2	++++	0.2
W-229-Au-001	0.6	0.6	0.55
W-230-Al-003	120	64	120
W-231-Mn-011-Poly	0.25	Processing	Processing

*	Ingots contain metal-rich inclusions due to consitutional supercooling.
**	Ingots regrown to remove metal-rich inclusions due to constitutional supercooling.
+	Pb dopant vaporized on two separate ingot growths.
++	No intentional impurity
+++	Heavy metals sensitivity of SSMS
***	Single growth probhibited due to excessive impurity doping for permanence studies.
++++	Atomic absorption analysis of ingot melt sample showed 2.8% Gd by weight of sample.

line at m/e = 98 1/2 was identifiable only on the first photoplate exposure. The above tang results show that the ingot seed concentration is closer to $3x10^{14}$ atoms/cm^3 at the point where 50% of the silicon charge had been consumed during ingot growth. This implies a Au segregation coefficient k_{Au} = $2.5x10^{-5}$ with the melt concentration at $1.2x10^{19}$ atoms/cm^3. This is in reasonable agreement with the value quoted in the literature,[4] k_{Au} = $5x10^{-5}$.

Multiple spark source analyses of Al-doped ingot W-230 yielded an average impurity concentration of $1.2x10^{17}$ atoms/cm^3. The heavy dopant concentration permitted the use of the Al^+ m/e = 27 photoplate line, yielding several exposures. This reduced the analytical errors that stem from using ionization factors greater than 1 which are associated with the Al^{++} and Al^{+++} lines. An Al segregation coefficient k_{Al} = $3x10^{-2}$ was obtained using the melt concentration of $4x10^{18}$ atoms/cm^3. This is in good agreement with the k_{Al} value determined in the earlier phases of the program.[1,2]

The k_{Al} calculated by using the ingot seed resistivity of 1.5 ohm-cm ($1x10^{16}$ atoms/cm^3) was $2.5x10^{-3}$. This lower k_{Al} is indicative of oxygen present in Czochralski pulled ingots. Oxygen-aluminum reactions tend to reduce the electrically active aluminum, producing the lower apparent segregation coefficient.[2]

The first Mn-doped polycrystalline ingot had a melt concentration of $5x10^{14}$ atoms/cm^3. We found numerous areas of fine grain structure in the seed end of the ingot due to inclusion-induced breakdown. An additional ingot was grown with Mn at $2.5x10^{14}$ atoms/cm^3 to render more reproducible and measurable solar cell efficiencies in subsequent polycrystalline wafers.

The Gd-doped ingot W-228 produced late in the last quarter was spark source analyzed early in this quarter. Three separate spark source mass spectrometer evaluations were performed on individual tang samples, all yielding a Gd concentration below the sensitivity of the mass spectrometer ($2x10^{14}$ atoms/cm^3). These data and the ingot dopant melt concentration of $1.8x10^{20}$ atoms/cm^3 imply $k_{Gd}<1x10^{-6}$.

A best estimate [3] of the impurity concentrations for the Phase IV ingots is listed in Table 3.

The resistivity and etch pit data for all of Phase IV ingots are indicated in Table 4. Etch pit analysis is not applicable to the polycrystalline samples.

As in the past carbon and oxygen concentrations of each odd numbered ingot were measured by infrared absorptionat room temperature using Fourier Transform Infrared Spectroscopy. The amplitudes of the absorption peaks at 605 cm^{-1} and 1107 cm^{-1} are proportional to the carbon and oxygen concentrations respectively. The calibration factors used in these evaluations are 2.2 $atoms/cm^2$ for carbon (2) and 4.9 $atoms/cm^2$ for oxygen.[5] Measured concentrations are listed in Table 5. Normal carbon and oxygen concentrations found in Czochralski grown material are in the range of 2.5 to $5x10^{17}$ $atoms/cm^3$ for carbon and 5 to $150x10^{16}$ $atoms/cm^3$ for oxygen.

3.2 Silicon Material Evaluation by Deep Level Spectroscopy

3.2.1 Analysis of Cr-Doped Polysilicon Ingots

In the last quarterly report[6] we showed preliminary data from polycrystalline ingotW216 containing $8x10^{14}$ cm^{-3} metallurgical concentration of Cr but only about $7x10^{12}$ cm^{-3} electrically-active Cr (as determined from DLTS measurements). Since then we have completed further DLTS measurements on this ingot which show that active Cr concentration indeed is very low and falls between 4 and $9x10^{12}cm^{-3}$, Table 6. The electrically-active Cr concentration in a single crystal, containing $8x10^{14}$ cm^{-3} total Cr is expected to be $\sim 1.8x10^{14}$ cm^{-3}. Ingot W216 however, contained inclusions which resulted in partial breakdown in the crystal structure and a large scatter in the cell performance which was in the range of 5 to 6% (uncoated).

To circumvent the ambiguity associated with the interpretation of the data due to inclusions, a second polycrystalline ingot, W-227, was grown with a lower Cr ($4.3x10^{14}$ cm^{-3}) concentration. This ingot

TABLE 3 . BEST ESTIMATE OF IMPURITY CONCENTRATIONS

Ingot Identification	Best Estimate of Impurity Conc. ($\times 10^{15}$ ATOMS/CM^3)
W-198-00-000	NA*
W-199-00-000	NA
W-200-V-004-Poly	0.38
W-201-Mo-007-Poly	0.003
W-202-Ti-013-Poly	0.018
W-203-V-005-Poly	0.05
W-204-Cr-008-Poly	0.82
W-205-Fe-009-Poly	0.61
W-206-V-006	0.026
W-207-Mo-008	0.002
W-208-Cr-009	0.19
W-209-Ti-014	0.02
W-210-Ti-015	0.10
W-211-Cu-007	1.8
W-212-Cu-008	12.5
W-213-Pb-001	ND+
W-214-V-007-Poly	0.4
W-215-Mo-009-Poly	0.002
W-216-Cr-010-Poly	1.0
W-217-Ta-005	0.0003
W-218-Ta-006	0.0001
W-219-V-008	0.009
W-220-W-005	0.0007
W-221-Ni-005	8.2

TABLE 3 BEST ESTIMATE OF IMPURITY CONCENTRATIONS (Continued)

Ingot Identification	Best Estimate of Impurity Conc. (x 10^{15} atoms/cm^3)
W-222-Ag-002	4.6
W-223-Ni-006	1.1
W-224-HSC/DCS057	++
W-225-Mn-009	1.5
W-226-Mn-010	***
W-227-Cr-011-Poly	0.4
W-228-Gd-001	0.4
W-229-Au-001	0.6
W-230-Al-003	120
W-231-Mn-011-Poly	Processing

*	Not applicable
+	ND - Non detectable
++	No intentional impurity
***	Single growth prohibited due to excessive impurity doping for permanence studies

TABLE 4 INGOT ELECTRICAL AND DEFECT CHARACTERISTICS

Ingot Identification	TGT Resistivity (ohm-cm)	Actual Resistivity (ohm-cm)	Etch Pit Density (/cm^2)
W-198-00-000	4.0	4.1-3.9	0-3K
W-199-00-000	4.0	3.7-3.5	1-5K
W-200-V-004/Poly	4.0	3.6-2.3	NA
W-201-Mo-007/Poly	4.0	3.8-2.3	NA
W-202-Ti-013/Poly	4.0	5.3-3.9	NA
W-203-V-005/Poly	4.0	4.4-3.8	NA
W-204-Cr-008/Poly	4.0	4.7-4.3	NA
W-205-Fe-009/Poly	4.0	4.0-3.2	NA
W-206-V-006	4.0	3.7-3.6	0-5K
W-207-Mo-008	4.0	3.8-3.5	0-15K
W-208-Cr-009	4.0	3.7-3.5	0-15K
W-209-Ti-014	4.0	4.0-3,3	0-10K
W-210-Ti-015	4.0	4.0-3.5	0-5K
W-211-Cu-007	4.0	4.0-3.1	0-5K
W-212-Cu-008	4.0	3.9-3.3	5-20K
W-213-Pb-001	4.0	3.3-2.7	10-20K
W-214-V-007-Poly	4.0	3.8-3.1	NA
W-215-Mo-009-Poly	4.0	3.8-1.7	NA
W-216-Cr-010-Poly	4.0	7.6-2.9	NA
W-217-Ta-005	4.0	3.5-3.0	0-10K
W-218-Ta-006	4.0	3.7-3.2	0-5K

TABLE 4 INGOT ELECTRICAL AND DEFECT CHARACTERISTICS (Continued)

Ingot Identification	TGT Resistivity (ohm-cm)	Actual Resistivity (ohm-cm)	Etch Pit Density (/cm^2)
W-219-V-008	4.0	3.6-3.3	0-5K
W-220-W-005	4.0	3.7-3.2	0.20K
W-221-Ni-005	4.0	3.5-3.1	OK
W-222-Ag-002	4.0	5.8-5.7	0-Gross Lineage
W-223-Ni-006	4.0	3.6-3.1	0-5K
W-224-HSC/DCS057	1.0	1.4-1.2	5-20K
W-225-Mn-009	4.0	5.5-3.5	0-5K
W-226-Mn-010	4.0	***	***
W-227-Cr-011-Poly	4.0	3.9-3.5	NA
W-228-Gd-001	4.0	5.4-5.1	0-Gross Lineage
W-229-Au-001	4.0	4.3-4.2	0-30K
W-230-Al-003	1.5	1.5-0.5	0-20K
W-231-Mn-011-Poly	4.0	4.4-3.1	NA

* Not applicable

*** Single growth prohibited due to excessive impurity doping for permanence studies.

TABLE 5 INGOT CARBON AND OXYGEN CONCENTRATIONS

Ingot Identification	Carbon Concentration ($\times 10^{16}$ atoms/cm^3)	Oxygen Concentration ($\times 10^{16}$ atoms/cm^3)
W-201-Mo-007-Poly	7.0	61
W-203-V-005-Poly	12	59
W-205-Fe-009-Poly	8.0	34
W-207-Mo-008	5.4	43
W-209-Ti-014	6.4	61
W-211-Cu-007	6.0	57
W-213-Pb-001	8.0	57
W-215-Mo-009-Poly	10.0	56
W-217-Ta-005	12.0	50
W-219-V-008	25.0	43
W-221-Ni-005	10.0	53
W-233-Ni-006	20.0	77
W-225-Mn-009	4.0	58
W-227-Cr-011-Poly	16.0	82
W-229-Au-001	7.3	80
W-231-Mn-011-Poly	13.0	38

was inclusion-free. Cell data from this ingot showed much less scatter. Table 7 shows a comparison of data from Cr-doped and uncontaminated single crystal and polycrystalline solar cells. The data indicate that the presence of $4x10^{14}$ cm^{-3} Cr in a polycrystalline solar cell degrades its short circuit current and the cell performance. Compared to an uncontaminated polysilicon cell, the average I_{SC} of the Cr-doped cell is lower by ∿ 3mA and the cell efficiency is about 1.5% less. In both contaminated and uncontaminated poly cells, the junctions were quite leaky, causing low fill factors. This leakage is attributed to electrically-active grain boundaries present in the depletion region.

The spectral response data, Figure 1, reveal that grain boundaries and Cr impurity each individually lower the red response appreciably. More important to note is that $4x10^{14}$ cm^{-3} Cr present in the polysilicon degrades the spectral response.

To gain deeper insight into the behavior of Cr in the polysilicon, DLTS measurements were performed at various locations across the surface of an unprocessed wafer. To do this, 30 mil diameter Ti-Au Schottky barrier diodes were fabricated and tested.[6] The data in Table 8 show that there is about an order of magnitude variation from place to place in active Cr concentration. This is in contrast to earlier results for Mo, Ti and V doped polysilicon wafers[8,9] where little or no variation was detected. Another noteworthy feature is that the active Cr concentration in single crystal silicon containing $4x10^{14}cm^{-3}$ Cr is ∿ $8x10^{13}$ cm^{-3}; but in this polysilicon ingot, it is 2-20 times smaller ($0.3\text{-}3x10^{13}cm^{-3}$). This is consistent with previous observations relating to Cr-doped poly-ingot 216 (Table 6). Again, however this result contrasts sharply to those for Mo, V and Ti doped polysilicon where the active impurity content was equal to that expected from single crystal data.

We may rationalize the above observations in the light of the high diffusion constant of Cr in silicon compared to those of Mo, V and Ti.[3] First, because Cr diffuses rapidly in silicon we might expect it to preferentially segregate to the grain boundaries and form metal-rich

TABLE 6

Active Cr Concentration in Polycrystalline Ingot-216 Containing 8×10^{14} cm^{-3} Cr.

SAMPLE ID	ACTIVE Cr CONCENTRATION (cm^{-3})
1-T	4.5×10^{12}
1-B	9.0×10^{12}
2-T	6×10^{12}
2-B	7×10^{12}
3-T	5×10^{12}
3-B	7×10^{12}
4-T	7.2×10^{12}
4-B	7.6×10^{12}

TABLE 7

Comparison of Uncontaminated Baseline and Cr-Contaminated Single Crystal and Polycrystalline Solar Cell Data

Ingot ID	I_{SC} (mA)	V_{OC} Volts	FF	Cell Efficiency (%)
003-Single Crystal Baseline	22.35	0.557	0.75	10.0
076-Polycrystal Baseline	19.23	0.505	0.66	6.9
072-Single Crystal Contaminated with 4×10^{14} cm^{-3} Cr	20.86	.491	.70	7.9
227-Polycrystal Contaminated with 4×10^{14} cm^{-3} Cr	16	.47	.66	5.26

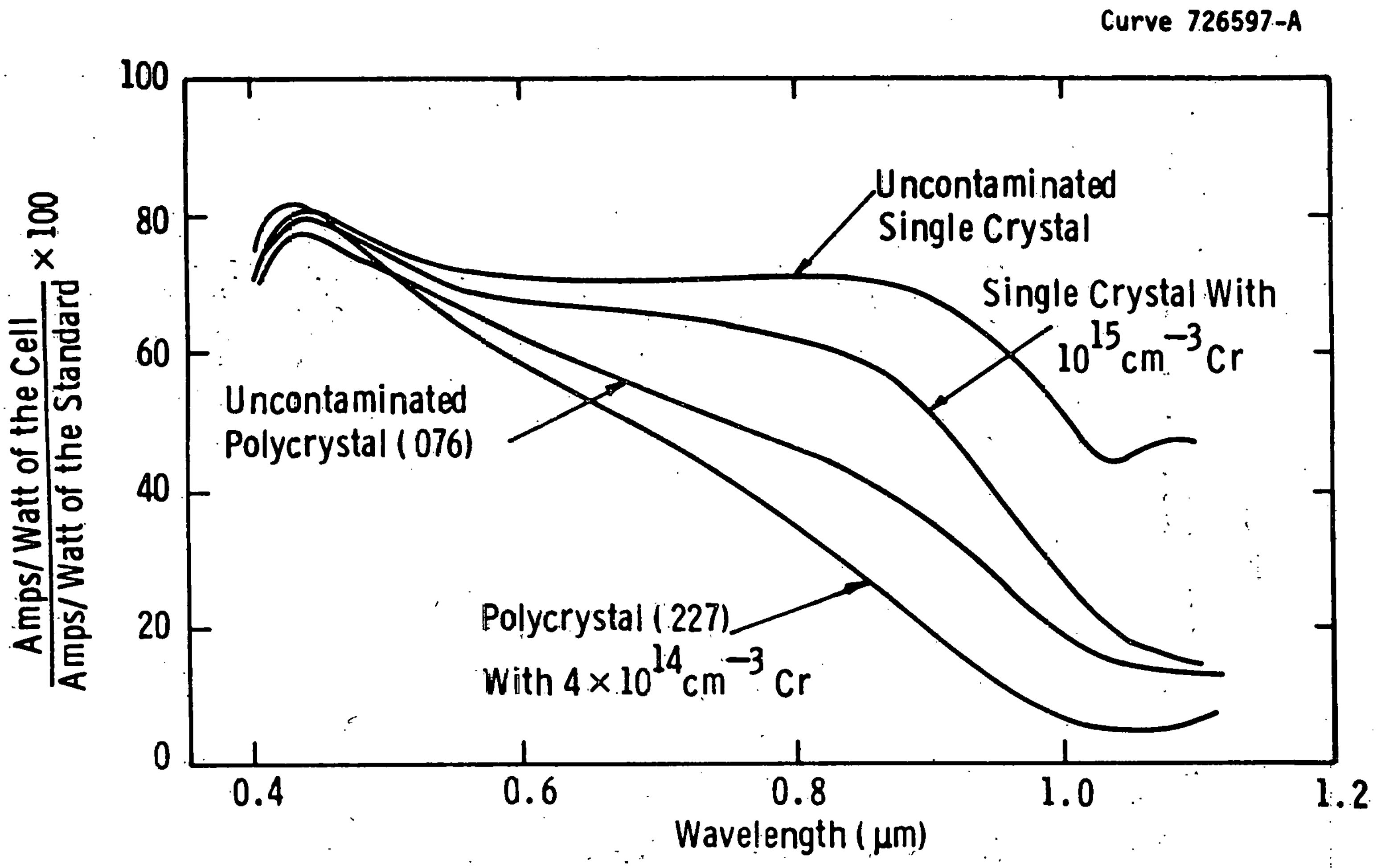

Figure [illegible] Spectral Response Data on Cr-doped Polycrystalline Solar Cells.

TABLE 8

Distribution of Active Cr Concentration across Polysilicon Wafers (Ingot-227) Containing a Metallurgical Cr Concentration of 4.0×10^{14} cm-3.

SAMPLE ID	ACTIVE CR CONCENTRATION (cm^{-3})
1 - T	2.9×10^{13}
1 - M	1.16×10^{13}
1 - B	1.37×10^{13}
2 - T	1.0×10^{13}
2 - M	9.40×10^{12}
2 - B	1.43×10^{13}
3 - T	5×10^{12}
3 - M	1.0×10^{13}
3 - B	1.10×10^{13}
4 - T	1.4×10^{13}
4 - M	1.6×10^{13}
4 - B	1.6×10^{13}
5 - T	1.7×10^{13}
5 - M	3.1×10^{12}
5 - B	3.8×10^{12}
6 - T	1.5×10^{13}
6 - M	8.6×10^{12}
6 - B	2.0×10^{13}

precipitates there. Grain boundaries provide a sink of low free energy sites for the defects and impurities. A large diffusion constant of Cr will result in diffusion and segregation of Cr into the grain boundaries from the adjacent grains while the crystal is cooling from the growth temperature. Since the average grain size was ∿ 1mm, crystal cooling time of 1 hr coupled with an average diffusion constant of 10^{-6} cm^2/sec during cooling will result in a diffusion distance of ∿ 1/2 mm ($x = \sqrt{Dt} = \sqrt{10^{-6}x3600} = 0.06$ cm). The diffusion constant of Cr in silicon at the temperatures of interest is not known exactly, although our gettering experiments (below) indicate that it diffuses much faster than Ti in Si. (Moreover the value for Cr should be in the range of those for Fe (4)). The diffusion constant of Ti in Si at 825°C is ∿ 10^{-11} cm^2/sec. Since a diffusion process gives rise to a concentration profile, it is not surprising that we observed an order of magnitude variation in the Cr concentration over the polysilicon wafer.

Another important conclusion that can be drawn from the DLTS data is that when Cr segregates into the grain boundaries it becomes electrically inactive, i.e. it does not give rise to the E_V+0.31eV trap; otherwise we would detect a higher active Cr concentration at or near the grain boundaries. Figure 2 shows the photomicrograph of the regions in which highest and lowest impurity concentrations were measured. At this magnification it is difficult to point out the impurity-grain boundary interaction. However, the diodes which showed lowest impurity concentration do show grain boundaries. Other diodes also show microstructural features, therefore, one can explain these data by the conjecture that all structural features do not provide an equally effective sink for Cr.

The cell data, particularly the drop in I_{SC}, and the red degradation in spectral response suggest an appreciable loss in carrier lifetime due to $4x10^{14}$ cm^{-3} Cr in the polysilicon. However, the DLTS measurements indicate that the concentration of active Cr in the starting wafer is only $0.3\text{-}3x10^{13}$ cm^{-3}, with an average of ∿ $1x10^{13}$ cm^{-3} If we use electrically active to metallurgical Cr ratio of 0.23 from the single crystal data[3] then $1x10^{13}cm^{-3}$ active Cr corresponds to a

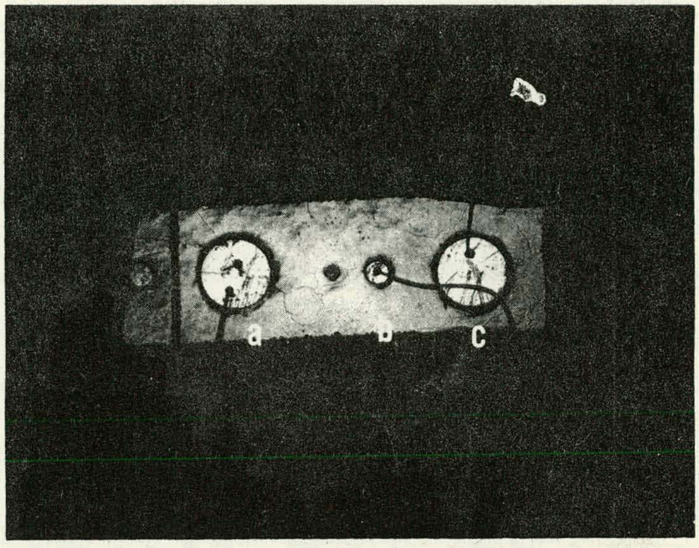

$a = 3.8 \times 10^{12}$, $b = 3.1 \times 10^{12}$, $c = 1.7 \times 10^{13}$

(a)

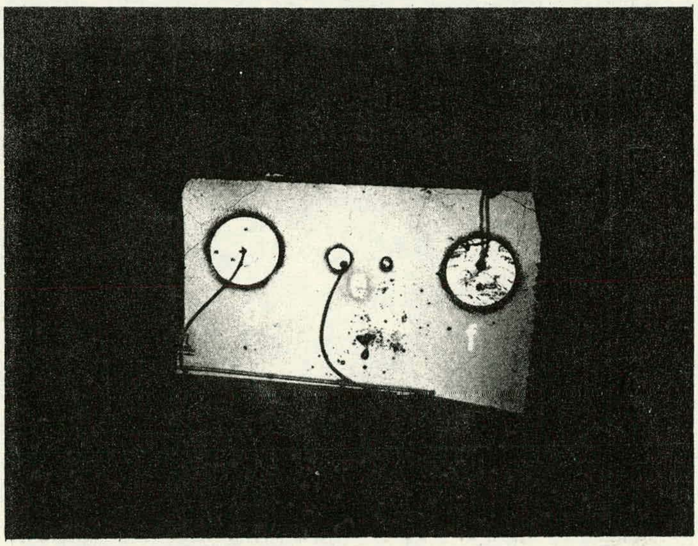

$d = 1.5 \times 10^{13}$, $e = 8.6 \times 10^{12}$, $f = 2.0 \times 10^{13}$

(b)

Figure 2 Microstructure of Cr-doped Polycrystalline Silicon Wafers.

metallurgical concentration of ∿ $5x10^{13}$, which is below the threshold for Cr-induced cell degradation.[1] This means that Cr-induced loss of carrier lifetime in polysilicon cannot be entirely accounted for by the electrically active average Cr. However, in certain areas the active Cr concentration is somewhat above the threshold. This anomaly can be explained by speculating that Cr which segregates into the grain boundaries somehow increases the recombination at the grain boundaries which in turn degrades the carrier lifetime.

We plan to rerun some of the solar cell experiments to test these ideas.

3.2.2 Analysis of Mo Gettering by $POC\ell_3$

Earlier we reported that $POC\ell_3$ gettering at 1100°C for 17 hours had no effect on Mo, indicating that the diffusion constant of Mo in silicon is very small.[3] In order to estimate the diffusion constant, we created a Mo out-diffusion profile via more intense gettering. We raised the $POC\ell_3$ gettering temperature to 1250°C (again 17 hours) for ingot Mo-077 containing $4x10^{12}$ cm^{-3} . After the gettering treatment we removed the n^+ region by etching. The interface location is accurate within $\pm$ 1 μm. The gettered wafers were then step-etched, and on each step Ti-Au Schottky barrier diodes were fabricated to determine the active Mo concentration by the DLTS method. The data in Table 9 show only weak evidence of Mo gettering even by this rather intense treatment, indicating that Mo cannot be appreciably extracted from silicon even at 1250°C. DLTS data for locations close to the junction were somewhat unclear and some more work is being done in that region.

3.2.3 Analysis of Cr Gettering by $POC\ell_3$

This study was conducted on Ingot W181-Cr containing $1x10^{15}$ cm^{-3} metallurgical Cr for which DLTS measurements on the as grown wafers showed $1x10^{14}$ cm^{-3} of Cr to be electrically active. After an 825°C/50 min $POC\ell_3$ gettering cycle the diffused (n+) region was removed and the remainder of the wafer was etched in steps ranging in depth from zero to

TABLE 9

The Electrically-active Mo Concentration in Bulk Silicon After 1250°C/17 hrs $POCl_3$ gettering of Ingot W-077 Containing $4x10^{12}$ cm^{-3} Mo.

Distance from the Surface (μm)	Active Mo Concentration (cm^{-3})
2	
4.4	
8	$1.4x10^{12}$
10	$2.0x10^{12}$
25	$2.75x10^{12}$
37.5	$2.75x10^{12}$

50µm below the surface. On each step Schottky-barrier diodes again were fabricated by evaporating Ti-Au contacts. DLTS measurements on these Schottky barrier diodes showed no detectable electrically-active Cr (the DLTS detection limit is $\sim 3\times10^{11}$ cm^{-3}) as deep as 2 mils below the n+p interface.

In order to reduce the gettering intensity a similar experiment was performed subsequent to a 600°C/1 hr $POC\ell_3$ gettering cycle. It was striking to note that again no electrically active Cr was detected as far as 2 mil below the n+p interface. These data suggest that either Cr diffuses out very rapidly in the presence of $POC\ell_3$ even at low temperatures or that it becomes electrically inactive. In order to answer this question we need to do gettering at lower temperature/shorter time or perform a straight heat treatment without the presence of $POC\ell_3$.

It is important to note that although no Cr was detected after 825°C/50 min $POC\ell_3$ gettering, there may still be some Cr present below the detection limit because there was about 20% loss in the cell performance due to Cr.

3.2.4 Analysis of the Effects of Al and Au on Silicon Solar Cells

Ingot W230 was grown with 1.2×10^{17} cm^{-3} Al resulting in a resistivity of 1.5 Ω-cm, corresponding to 1×10^{16} cm^{-3} Al at the acceptor or substitutional sites. It is noteworthy that unlike boron, more than an order of magnitude Al is in some configuration where it does not act like dopant, but could give rise to deep levels.

The solar cells fabricated from this material, Table 10, indeed show an appreciable loss in the cell performance associated with a drop in the red response of the cells, Figure 3. Two deep levels, at E_V+0.44eV and E_V+0.49eV were detected by DLTS.

Gold is well known to be detrimental in silicon. However, most of the studies of Au in silicon were conducted by diffusing Au into Si. We have produced an ingot in which 5.5×10^{14} cm^{-3} Au was incorporated during the crystal growth. The data in Table 10 show that Au had a significant impact on the cell efficiency and the short circuit

TABLE 10

Solar Cell Data from Devices Fabricated on Single Crystals Contaminated with $4\text{x}10^{14}$ cm^{-3} Au (Ingot 229) and $1.2\text{x}10^{17}$ cm^{-3} Aℓ (Ingot 230).

Ingot ID	I_{SC}	V_{OC}	FF	Cell Efficiency
198-Baseline	21.75	.55	.74	9.34
229-Au	18.02	.502	.66	6.37
230-Aℓ	15.76	.501	.66	5.5

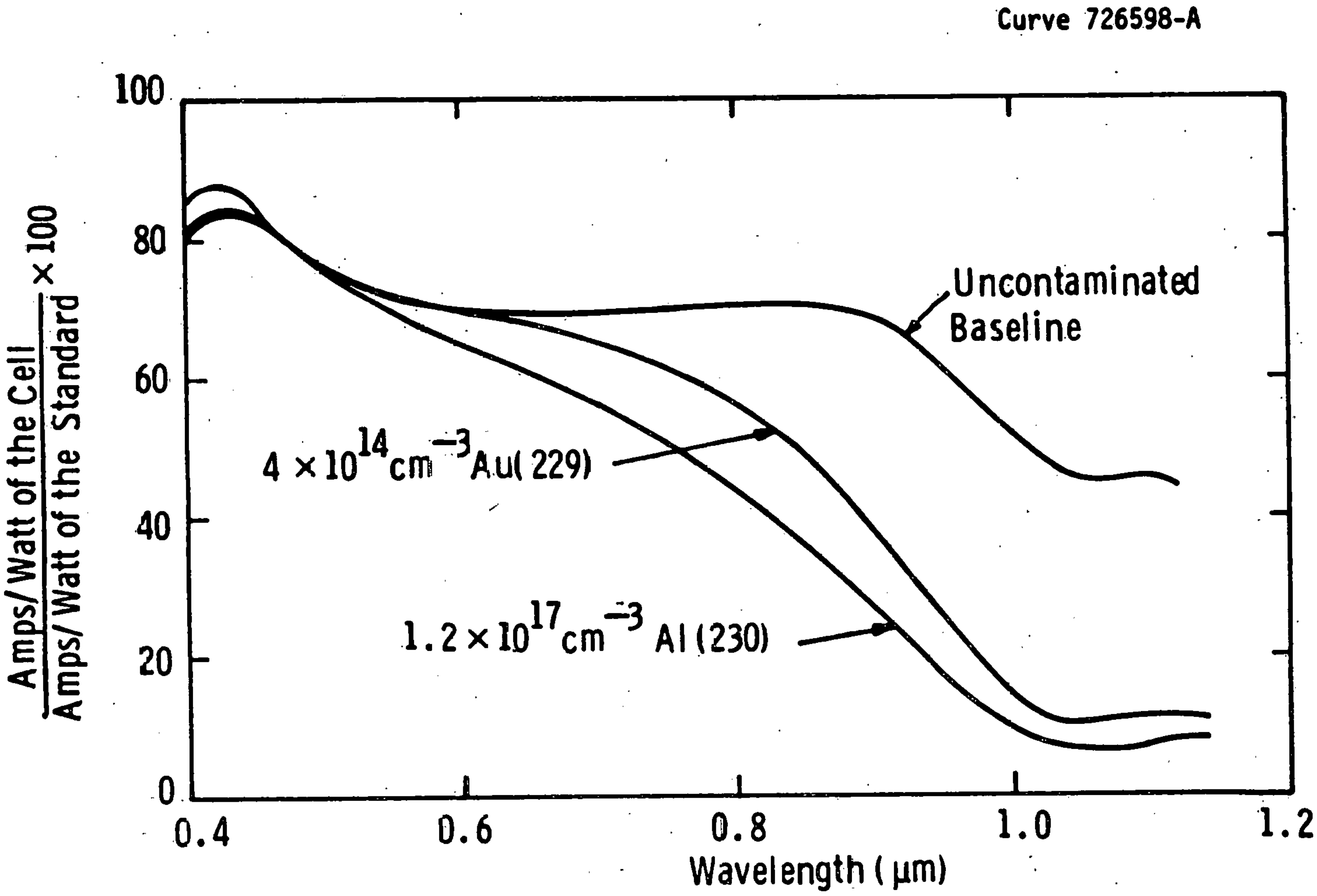

Figure 3 Red Response of Al-doped Solar Cells and Au-doped Solar Cells.

current indicating a decrease in minority carrier lifetime. This can also be seen from the significant drop in the red response of the cell, Figure 3. The DLTS results support the above observation since four deep levels, at E_V+0.22eV, E_V+0.34eV, E_V+0.47eV and E_V+0.53eV, were detected and their concentrations were 3.2×10^{13} cm^{-3}, 5.4×10^{13} cm^{-3}, 7.3×10^{12} cm^{-3} and 7.3×10^{12} cm^{-3}, respectively. In gold-diffused Si other investigators have detected levels at $E_V\pm$0.35eV and E_V+0.55eV. However, when gold is grown in we observe two extra levels. Another noteworthy feature of the data is that only a fraction of total gold is electrically active.

3.2.5 Solar Cell and Material Evaluation by DLTS

We have continued to monitor the electrically-active impurity concentrations of representative wafers (as grown) and solar cells to correlate device and materials effects due to impurities. Table 11 is a summary of current information collected by deep level transient spectroscopy for single and polycrystalline ingots. As before we did not detect any levels for Cu, Ta, Ag, Ni, Mn. However, deep levels due to Au and Al were detected. This compilation will be updated as the study continues.

TABLE 11

DLTS RESULTS ON IMPURITY-DOPED INGOTS

Ingot ID	Best Estimate of Metallurgical Impurity Concentration (N_M)	Active Impurity Concentration (cm^{-3})		
		In the Wafer N_{TW}	In the Cell (near junction) N_{TC}	$\frac{N_{TW}}{N_M}$
V-200-Poly	$4x10^{14}$	$1.3x10^{14}$	no data	0.32
Ti-202-Poly	$2x10^{13}$	$1.12x10^{13}$	$1.15x10^{12}$	0.56
V-203-Poly	$4x10^{13}$	$1.7x10^{13}$	undetectable	0.34
206-V	$2.6x10^{13}$	$6.43x10^{12}$	undetectable	0.25
207-Mo	$2.0x10^{13}$	$2.2x10^{12}$	$9x10^{11}$	1.1
208-Cr	$1.9x10^{14}$	$3.91x10^{13}$	undetectable	0.21
209-Ti	$2.0x10^{13}$	$8.12x10^{12}$	$1.15x10^{12}$	0.40
210-Ti	$1.0x10^{14}$	$2.91x10^{13}$	$3.6x10^{12}$	0.30
211-Cu	$1.8x10^{15}$	undetectable	undetectable	-
212-Cu	$1x10^{16}$	undetectable	undetectable	-
214-V-Poly	$2x10^{14}$	$6x10^{13}$	no data	0.30
215-Mo-Poly	$2.5x10^{12}$	$4.5x10^{12}$	no data	1.8
216-Cr-Poly	$8x10^{14}$	$7.5x10^{12}$	no data	.009
217-Ta	$1.5x10^{11}$	undetectable	no data	-
218-Ta	$6.5x10^{10}$	undetectable	no data	-
222-Ag	$4.5x10^{15}$	undetectable	undetectable	-
223-Ni	$1.0x10^{15}$	undetectable	undetectable	-
225-Mn	$1.0x10^{15}$	undetectable	undetectable	-
227-Cr-Poly	$4.0x10^{14}$	$1.2x10^{13}$(average)	no data	0.03
228-Gd	-	undetectable	no data	-
229-Au	$6.0x10^{14}$	$8x10^{13}$	no data	0.13
230-Al	$1.2x10^{17}$	$2x10^{12}$	no data	0.000016

3.3 The Permanence of Impurity Effects in Silicon Solar Cells

3.3.1 Temperature Effects

Experimental evidence[1-3] shows that solar cell performance depends upon both material quality and device process history. The operating life of a solar cell array in the field should exceed twenty years, so it is important to understand what effects specific impurities will have on long term efficiencies.

The time period of interest is extremely long compared to practical test times, so extrapolations from accelerated aging tests must be used to estimate long term solar cell performance. On the basis of earlier results and fundamental considerations, temperature is believed to be the dominant parameter affecting gradual cell degradation. A series of experiments has been underway[3,6,9] to determine the magnitude of the temperature-dependent degradation mechanisms for individual impurities.

3.3.1.1 Experimental Method

As noted before, prediffused silicon wafers containing single impurities are soaked at elevated temperatures for various lengths of time. These wafers are then further processed into test cells and their characteristics are measured. The rate of degradation of efficiency is determined at each temperature, assuming that, at least in the initial stages, cell efficiency decreases linearly with time. A linear least squares fit to the efficiency-time data gives estimates of the η_o (the initial efficiency) and $(1/\eta_o)\ d\eta/dt$ (the normalized rate of change of efficiency). From these parameters, determined for different temperatures, an Arrhenius plot is developed to express the temperature-time dependence of efficiency degradation for a particular impurity.

3.3.1.2 Experimental Results

The behavior of the ingots listed in Table 12 has been previously reported.[3,9]

TABLE 12

INGOTS USED IN PERMANENCE STUDIES

Ingot Identification	Impurity Concentration (cm^{-3})
W09700000	Baseline
W077Mo001	4.2×10^{12} Mo
W123Ti008	1×10^{14} Ti
W072Cr005	4×10^{14} Cr
W192Ag001	2.2×10^{15}
W183Nb002	$< 9\times10^{12}$ Nb
W135Fe005	7.8×10^{14} Fe
W166Fe007	1.06×10^{15} Fe
W167Nb001	$< 4.4\times10^{13}$ Nb
W211Cu007	1.8×10^{15} Cu

During this quarter, accelerated aging experiments were completed on ingots W221Ni005 ($8.2\text{x}10^{15}$ cm^{-3}) and W222Ag002 ($4.6\text{x}10^{15}$ cm^{-3}). For the nickel-doped silicon, the measured rates of cell degradation were $2.4\text{x}10^{-4}$ hr^{-1}, $4.5\text{x}10^{-3}$ hr^{-1}, and $1.7\text{x}10^{-2}$ hr^{-1} at 400, 600, and 800°C, respectively. These data, when fitted to an Arrhenius model, yield

$$\frac{1}{\eta_o}\frac{d\eta}{dt} = 28.47 \exp\left(-0.673\text{eV}/kT\right) \text{hr}^{-1}.$$

If cell failure is defined as a decrease to 90% of the initial cell efficiency, then based upon the above relationship, the predicted times to failure at possible operating temperatures are those given in Table 13.

For typical array temperatures no impurity-induced effects are expected during a twenty year lifetime.

For the silver-doped silicon, the experimental data were widely scattered and a fit to an Arrhenius model could be obtained only by regarding some of the data points as anomalous and disregarding them. When this is done, the measured normalized rates of cell degradation are $2.15\text{x}10^{-3}\text{hr}^{-1}$, $1.83\text{x}10^{-2}\text{hr}^{-1}$, and $3.85\text{x}10^{-2}\text{hr}^{-1}$ at 400, 600, and 800°C respectively. These rates, fitted to an Arrhenius model, yield

$$\frac{1}{\eta_o}\frac{d\eta}{dt} = 0.29 \exp\left(-0.37\text{eV}/kT\right) \text{hr}^{-1}.$$

Predicted time to failure at possible operating temperatures are then as shown in Table 14.

These predicted times to failure imply a very serious problem may exist for the use of silver-contaminated silicon. Because of the questionable validity of some of the data used in obtaining these projections, further investigation of silver-doped silicon should be undertaken to clarify the results.

TABLE 13

Predicted Time to Failure for Solar Cells Containing 8.2×10^{15} cm^{-3} Nickel Impurity

Operating Temperature, °C	Time to Failure (yr)
100	490
125	133
150	42
175	15
200	6

TABLE 14

Predicted Time to Failure for Solar Cells Containing 4.6×10^{15} cm^{-3} Silver Impurity

Operating Temperature, °C	Time to Failure, (yrs)
100	4.1
125	2.0
150	1.0
175	0.59
200	0.35

3.3.2 Electrical Bias Effects

The purpose of this experiment is to determine whether electrical bias coupled with moderate temperatures in operating solar cells may, over long periods of time, affect cell efficiency. The possible interactions between electric field and impurities in the solar cell junction region are not well understood and their effects must be determined empirically.

In these experiments, base line cells and cells containing one of several representative impurities are operated at a current density of 30 mA/cm^2; current is externally supplied by a constant current supply. In order to enhance and accelerate any electric field/impurity interactions which may occur, the cells are operated at elevated temperature. Silicon materials incorporated in this study are listed in Table 15.

Solar cell operation for periods of 100 hours have now been carried out at ten different temperatures. The experiment plan calls for further tests at increasingly higher temperatures until definite evidence of cell efficiency degradation is observed.

Average relative cell efficiency of the base line (no intentional impurity) cells after each temperature-bias exposure is plotted in Figure 4. This represents any cell degradation which is attributable to effects other than specific impurity effects. The average relative cell efficiencies of the impurity-doped cells, normalized to the base line cell behavior, are shown in Figures 5 to 12.

Clearly, the degradation at temperatures up to 225°C is small, usually less than 10%. No systematic effect is observable in these data, so tests are continuing at higher temperatures.

3.4 Thermochemical Gettering

A previous report[3] described the effects of some thermochemical processes which can be performed on single crystal silicon in order to mitigate the harmful effects of metal contamination. The thermochemical processes studied were (1) $POC\ell_3$ gettering, (2) $HC\ell$

TABLE 15

SILICON MATERIALS UNDERGOING ELECTRICAL BIAS TESTING

Ingot No.	Impurity
W-198-00-000 Baseline	None
W-166-Fe-007	Fe 1.06×10^{15}
W-167-Nb-001	Nb $<0.044 \times 10^{15}$
W-192-Ag-001	Ag 2.20×10^{15}
W-181-Cr-006	Cr 1.04×10^{15}
W-016-Fe-001	Fe 0.4×10^{15}
W-056-Cu-005	Cu 65×10^{15}
W-183-Nb-002	Nb $<0.009 \times 10^{15}$
W-123-Ti-008	Ti 0.105×10^{15}

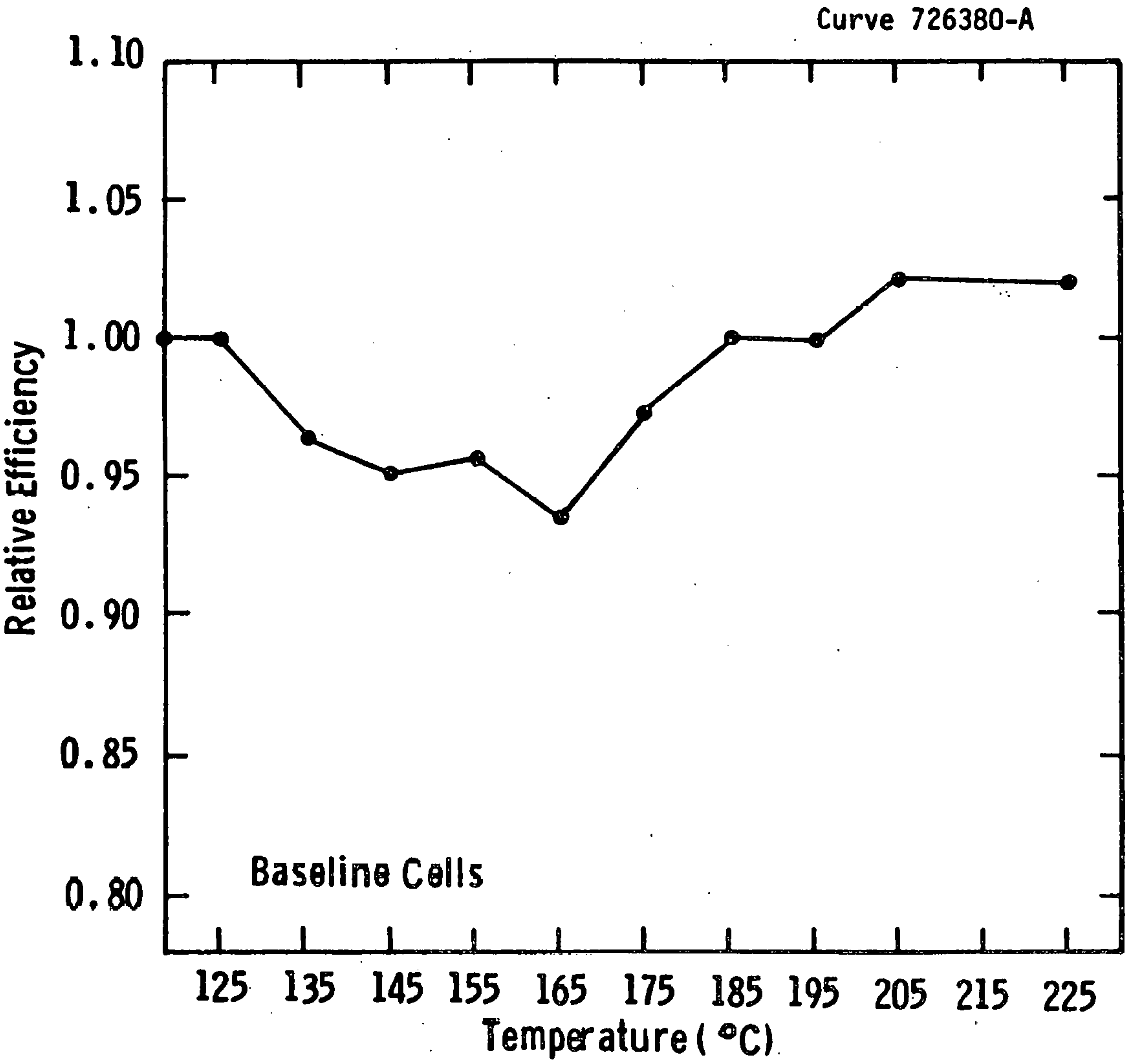

Figure 4 Effect of Electrical Bias on Relative Efficiency as a Function of Stress Temperature—Baseline Cells.

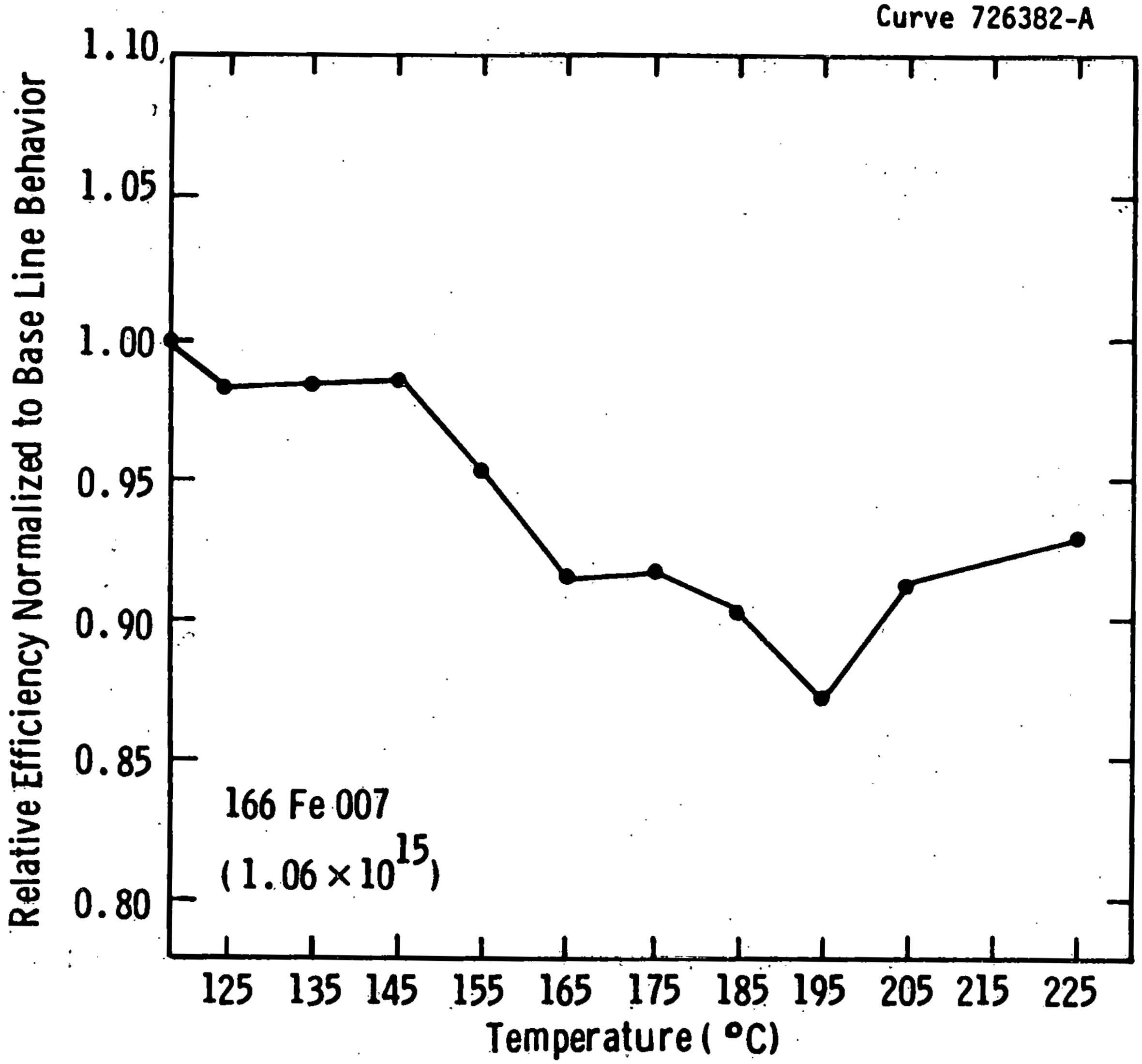

Figure 5 Effect of Electrical Bias on Relative Efficiency as a Function of Stress Temperature—Fe-doped (1.06×10^{15} cm^{-3}) Cells.

Curve 726377-A

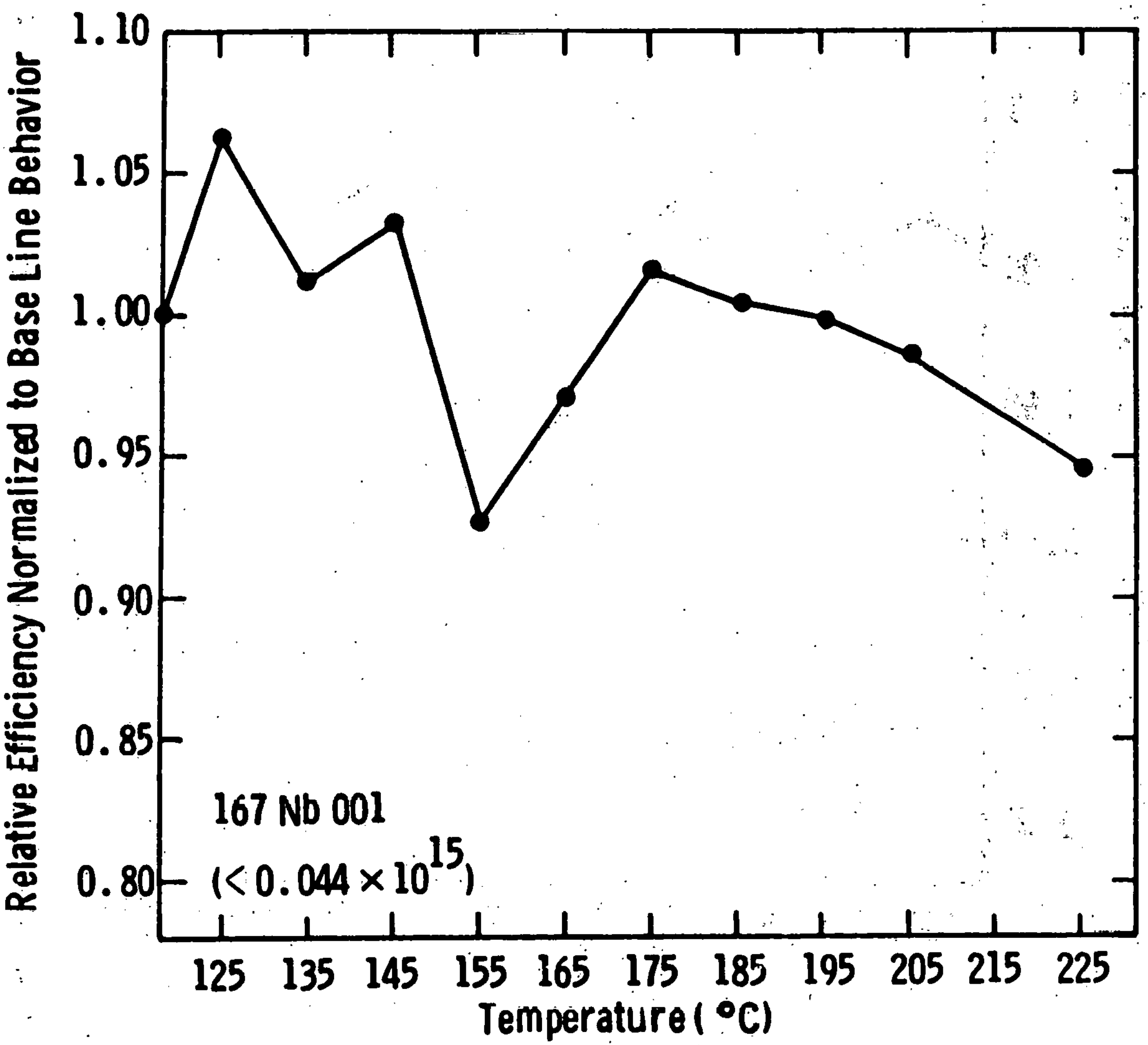

Figure 6 Effect of Electrical Bias on Relative Efficiency as a Function of Stress Temperature—Nb-doped ($<0.44 \times 10^{15} cm^{-3}$) Cells.

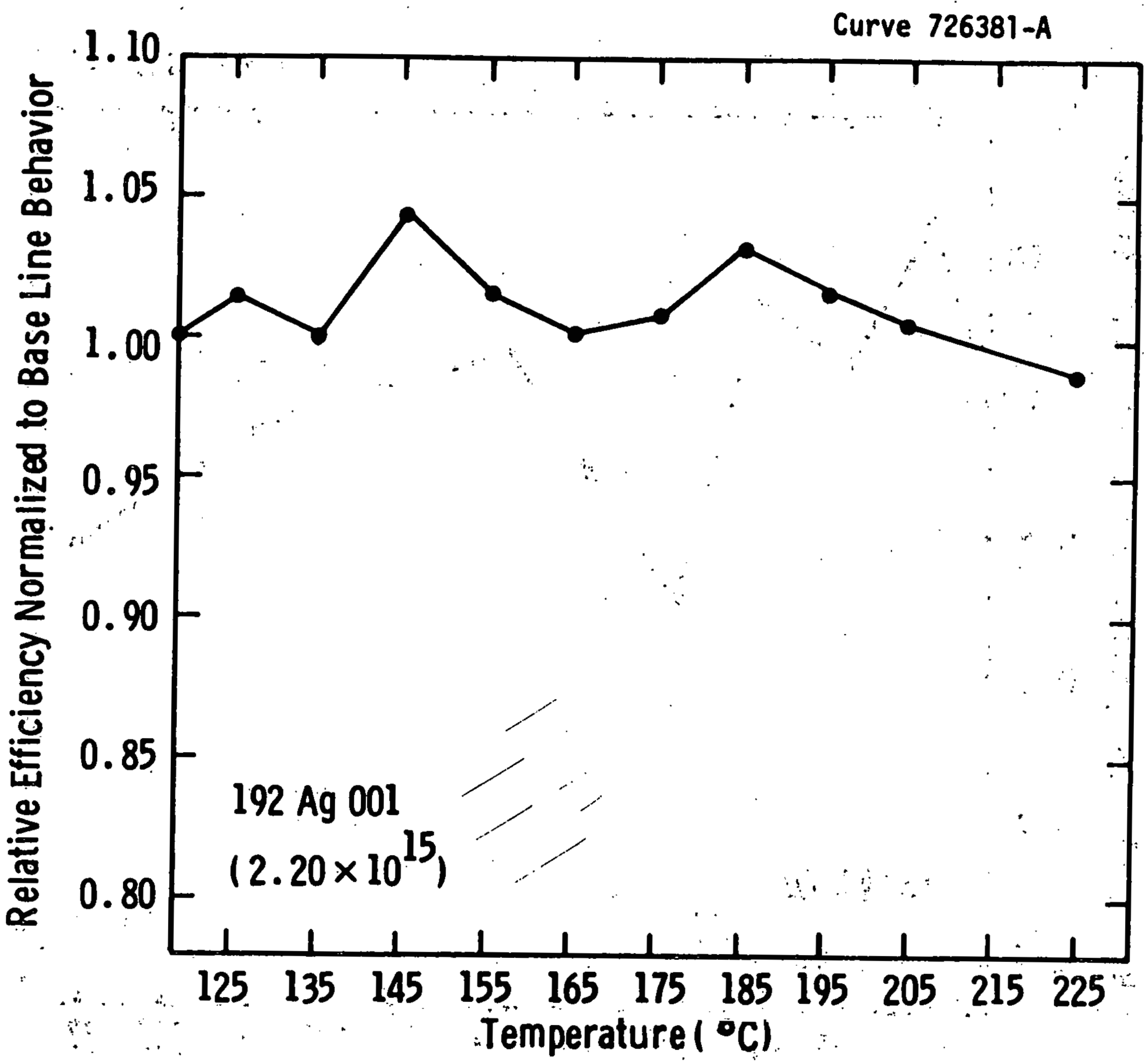

Figure 7 Effect of Electrical Bias on Relative Efficiency as a Function of Stress Temperature—Ag-doped ($2.20x10^{15}cm^{-3}$) Cells.

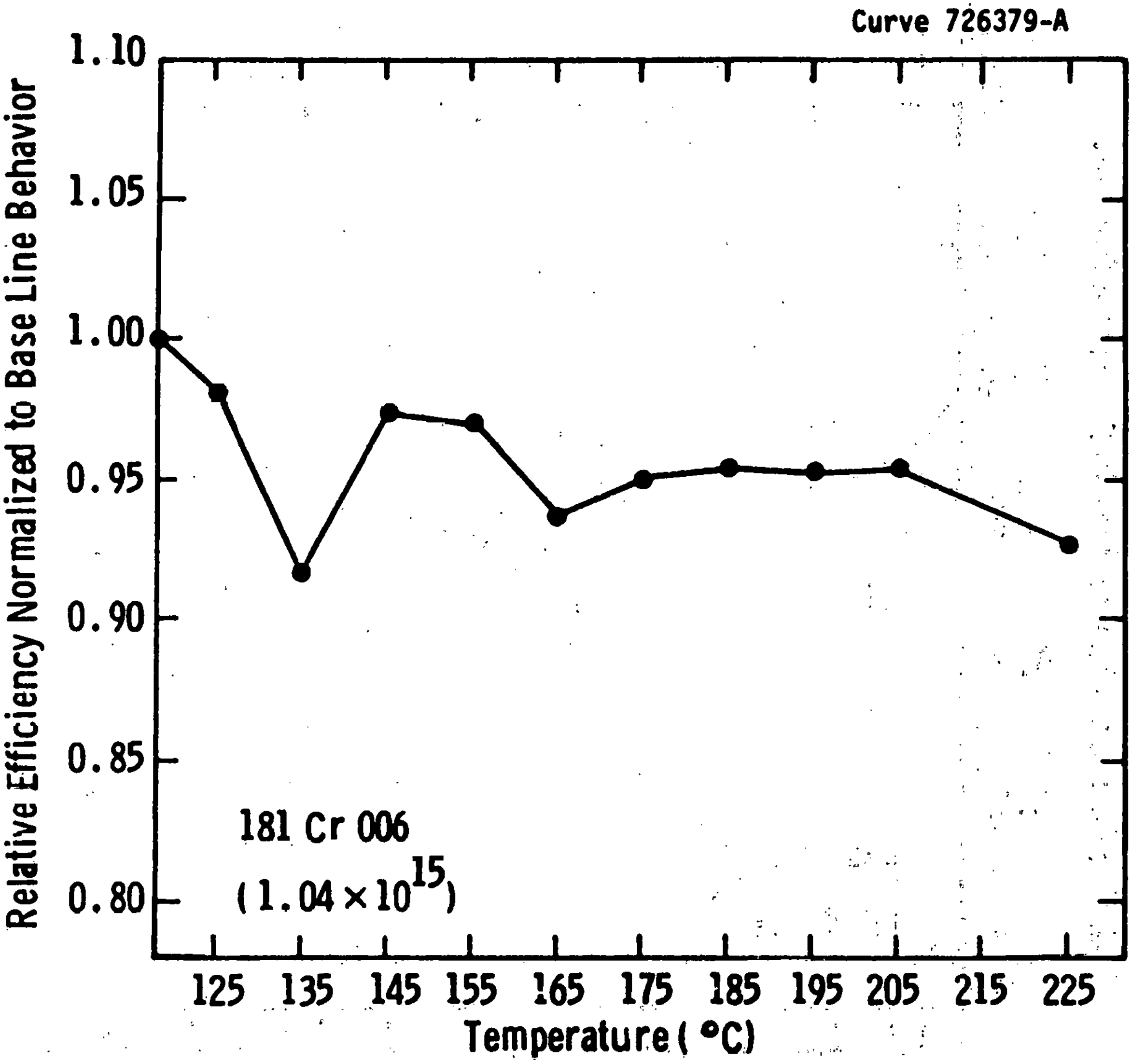

Figure 8 Effect of Electrical Bias on Relative Efficiency as a Function of Stress Temperature—Cr-doped ($1.04 \times 10^{15} cm^{-3}$) Cells.

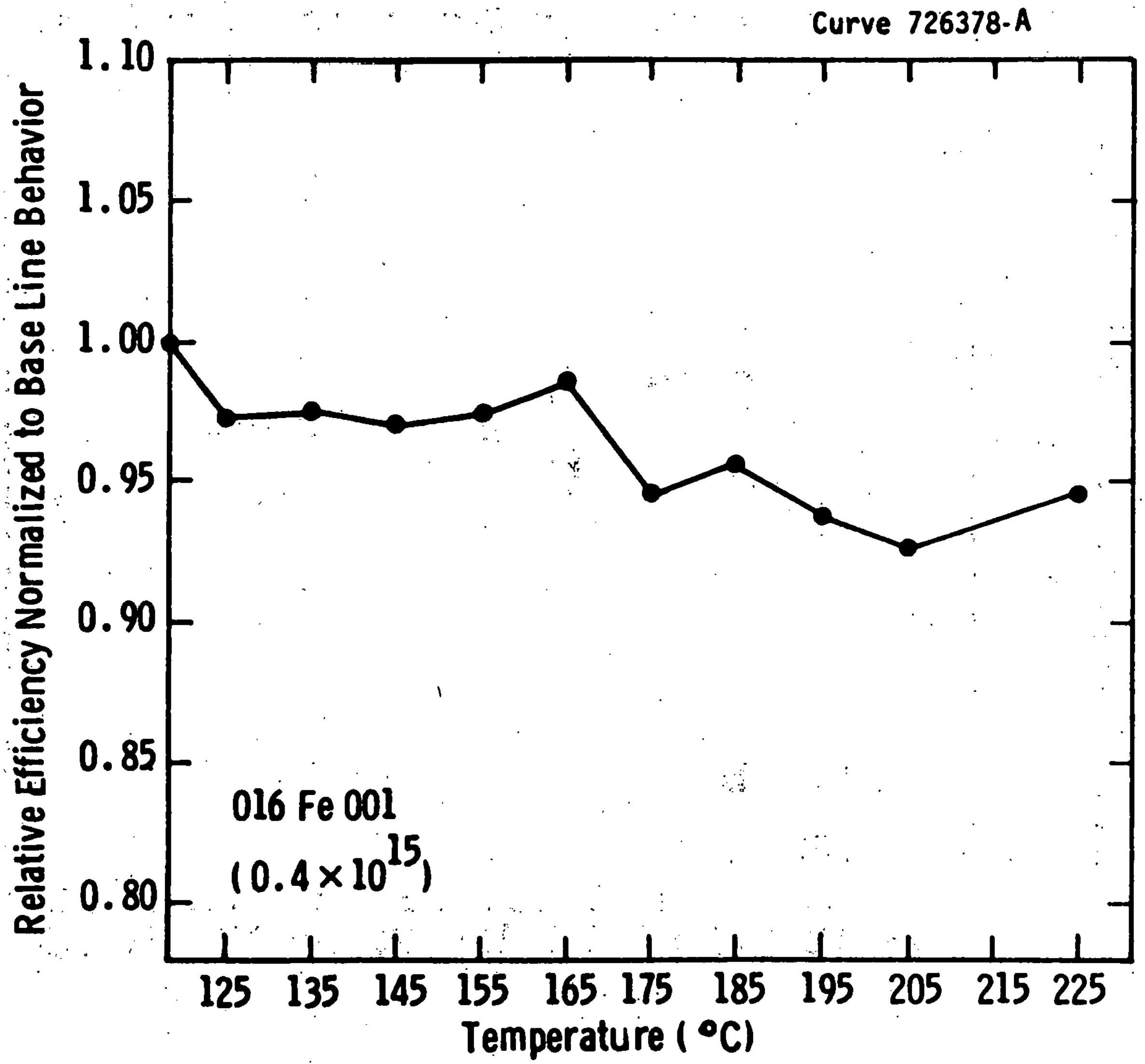

Figure 9 Effect of Electrical Bias on Relative Efficiency as a Function of Stress Temperature— Fe-doped ($0.4 \times 10^{15} cm^{-3}$) Cells.

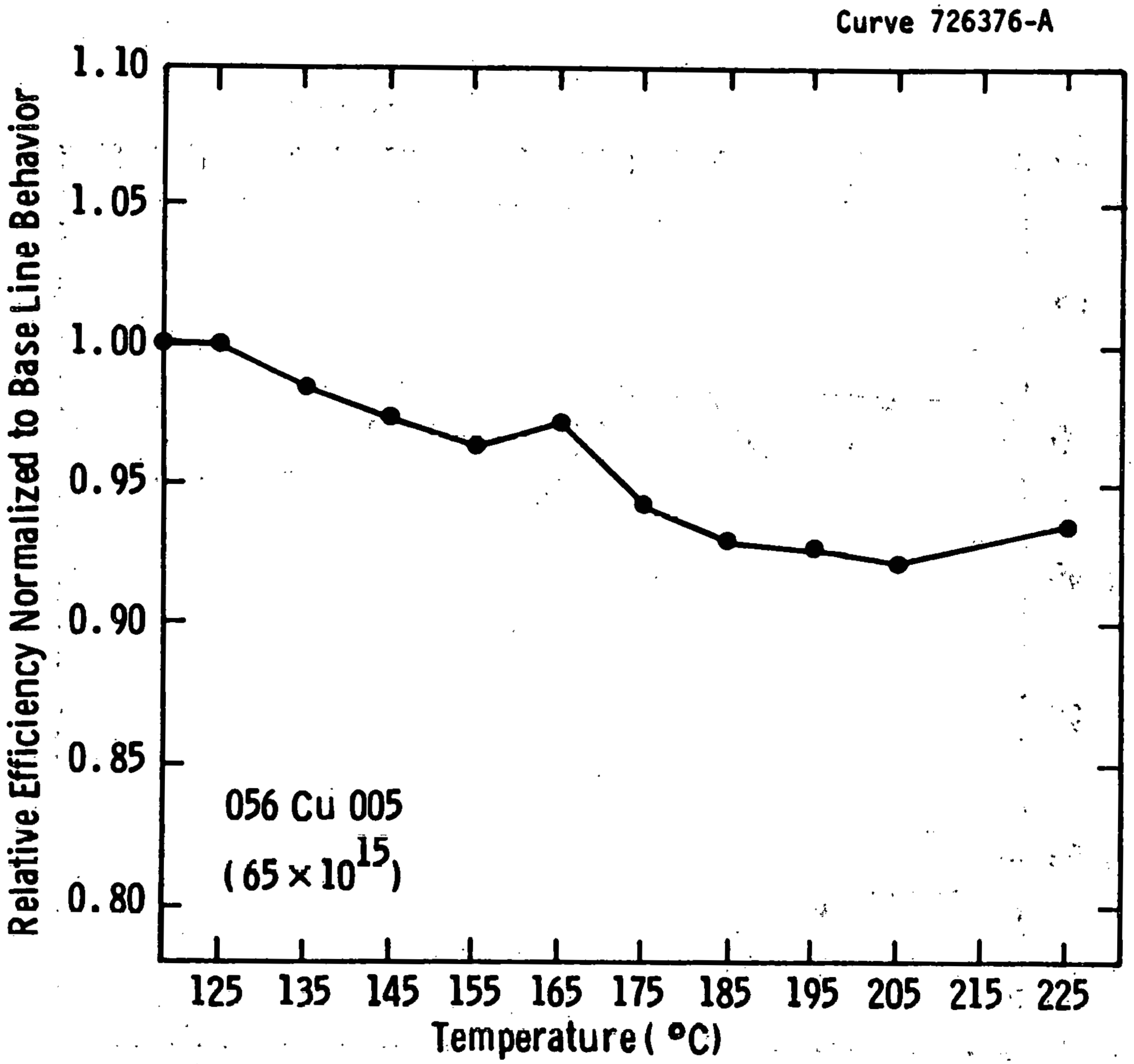

Figure 10 Effect of Electrical Bias on Relative Efficiency as a Function of Stress Temperature—Cu-doped (65x10^{15}cm^{-3}) Cells.

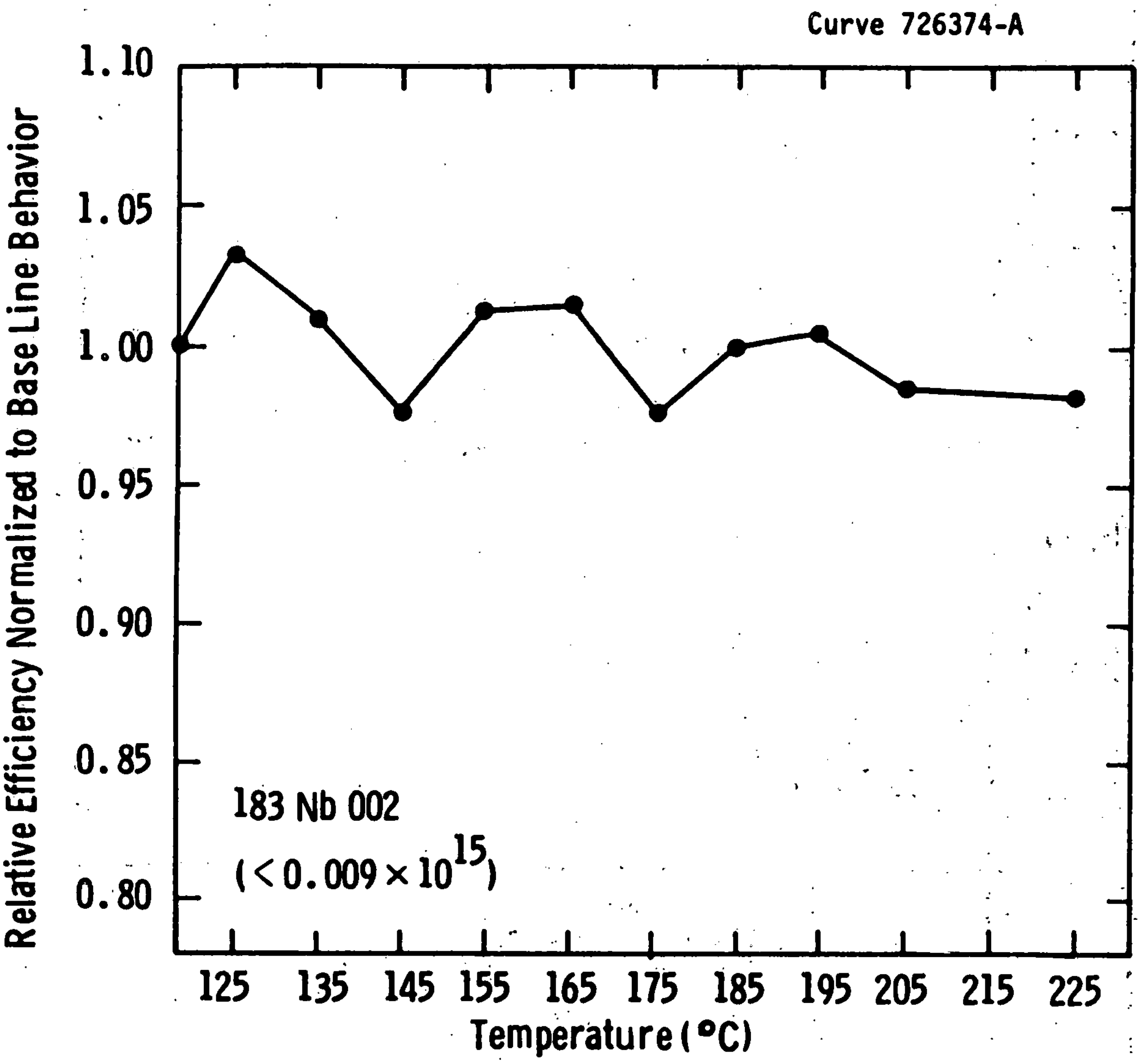

Figure 11 Effect of Electrical Bias on Relative Efficiency as a Function of Stress Temperature—Nb-doped ($<0.009 \times 10^{15} cm^{-3}$) Cells.

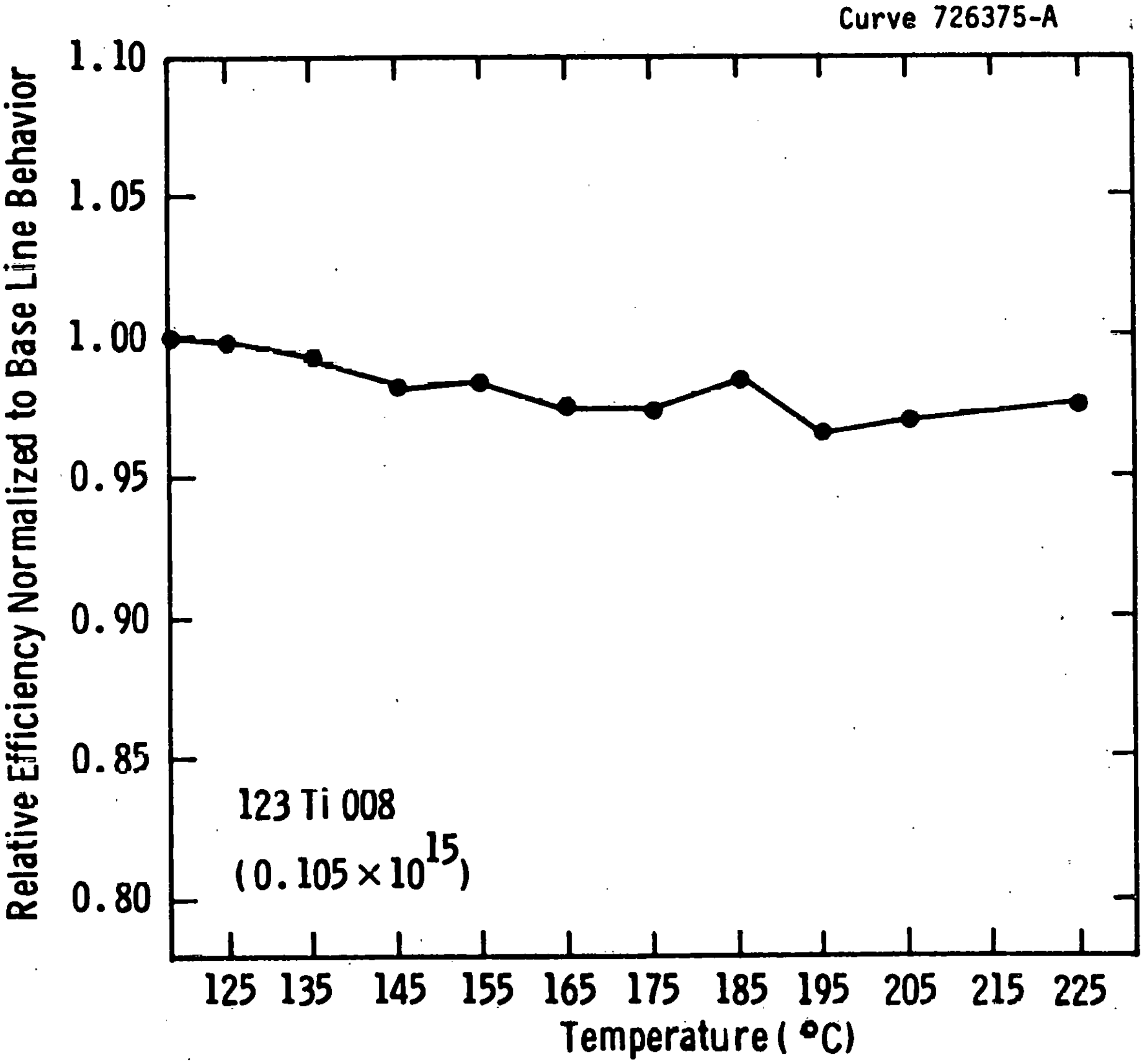

Figure 12 Effect of Electrical Bias on Relative Efficiency as a Function of Stress Temperature—Ti-doped ($0.105 \times 10^{15} cm^{-3}$) Cells.

gettering of <u>polycrystalline</u> silicon and of Cu-contaminated single crystal silicon.

The effects of $POC\ell_3$ gettering for periods of one hour at temperatures of 950°, 1000°, and 1100°C are illustrated in Figure 13. The data indicate that titanium and vanadium can be gettered from polycrystalline silicon, resulting in an increase in cell efficiency. However, the efficiency of cells made with polycrystalline material will still be low relative to single crystal material. Molybdenum is known to diffuse only very slowly in silicon; and this property is reflected in Figure 13, where it is apparent that molybdenum is not gettered to any observable extent from polycrystalline silicon under these test conditions.

The copper-doped <u>single</u> crystal material was only marginally inferior in cell performance to baseline material,[3] and therefore the $POC\ell_3$ gettering had little effect on cell efficiency, although it can be presumed that copper, a fast diffuser, was effectively gettered by the treatment.

The results of $HC\ell$ gettering for one hour at 1000° or 1100°C respectively is illustrated in Figure 14. Again, the more rapidly diffusing elements titanium and vanadium are effectively gettered from polycrystalline silicon, while slower diffusing molbydenum is not. Gettering of copper from single crystal silicon by $HC\ell$ treatment appears to be extremely effective. (However, a part of this apparent effectiveness is due to anomalously low cell efficiencies observed following the 1000°C $HC\ell$ treatment.

Further thermochemical processing experiments are in progress. In one of these, the effectiveness of argon implantation damage gettering combined with $HC\ell$ and $POC\ell_3$ gettering is being evaluated on copper-doped and titanium-doped solar cell material. Another experiment in progress will investigate the possibility that the p-n junction-forming step ($POC\ell_3$ diffusion) alone is sufficient to getter some harmful impurities from the junction region. Cells with ion implanted junctions (no anticipated gettering action) will be compared to cells made with the

Curve 726580-A

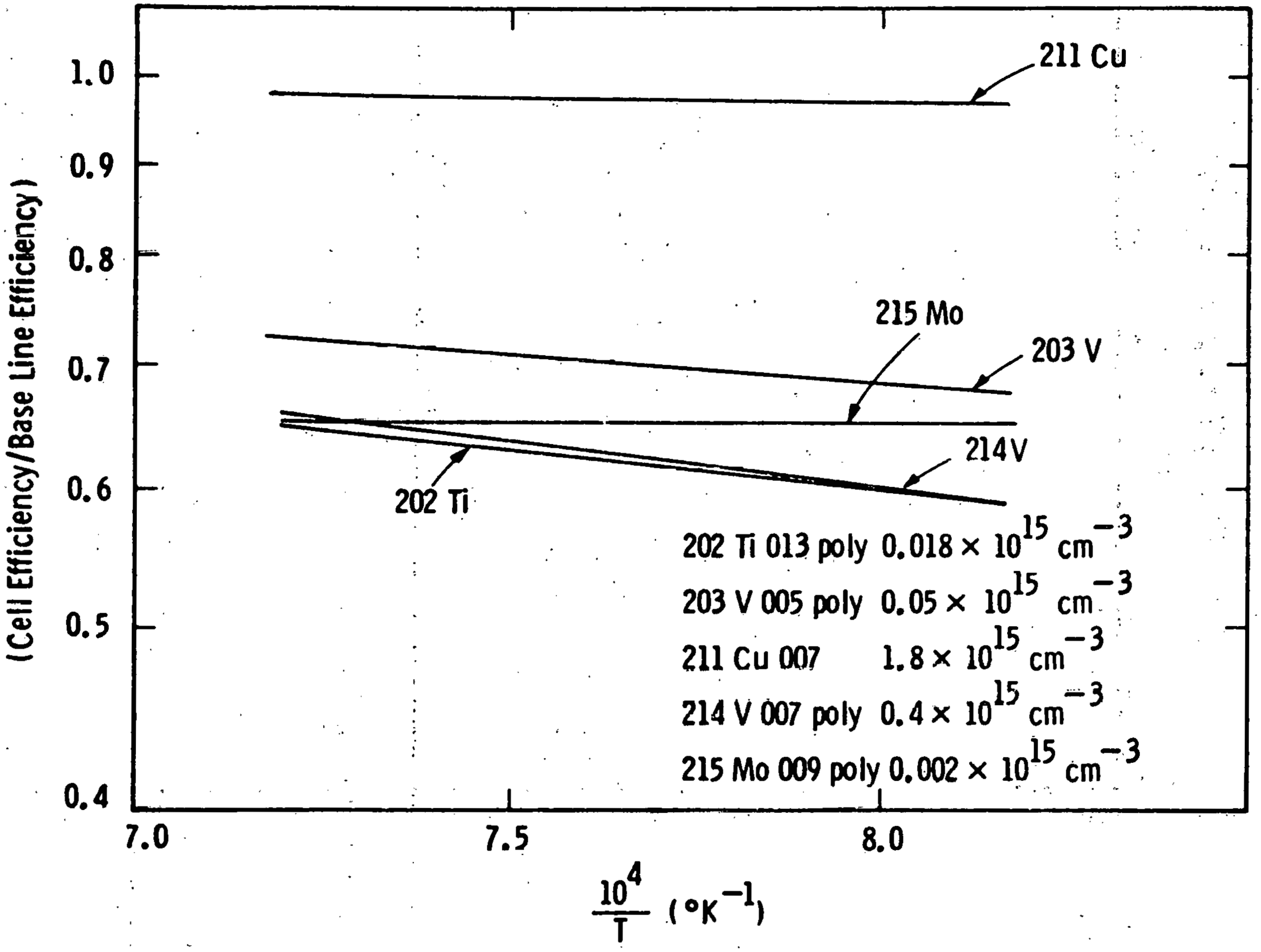

Figure 13 Gettering of Titanium, Vanadium, and Molybdenum from Polycrystalline Silicon, and of Copper from Single Crystal Silicon, by POCℓ_3 treatment at 940, 1000, and 1100°C.

Curve 726579-A

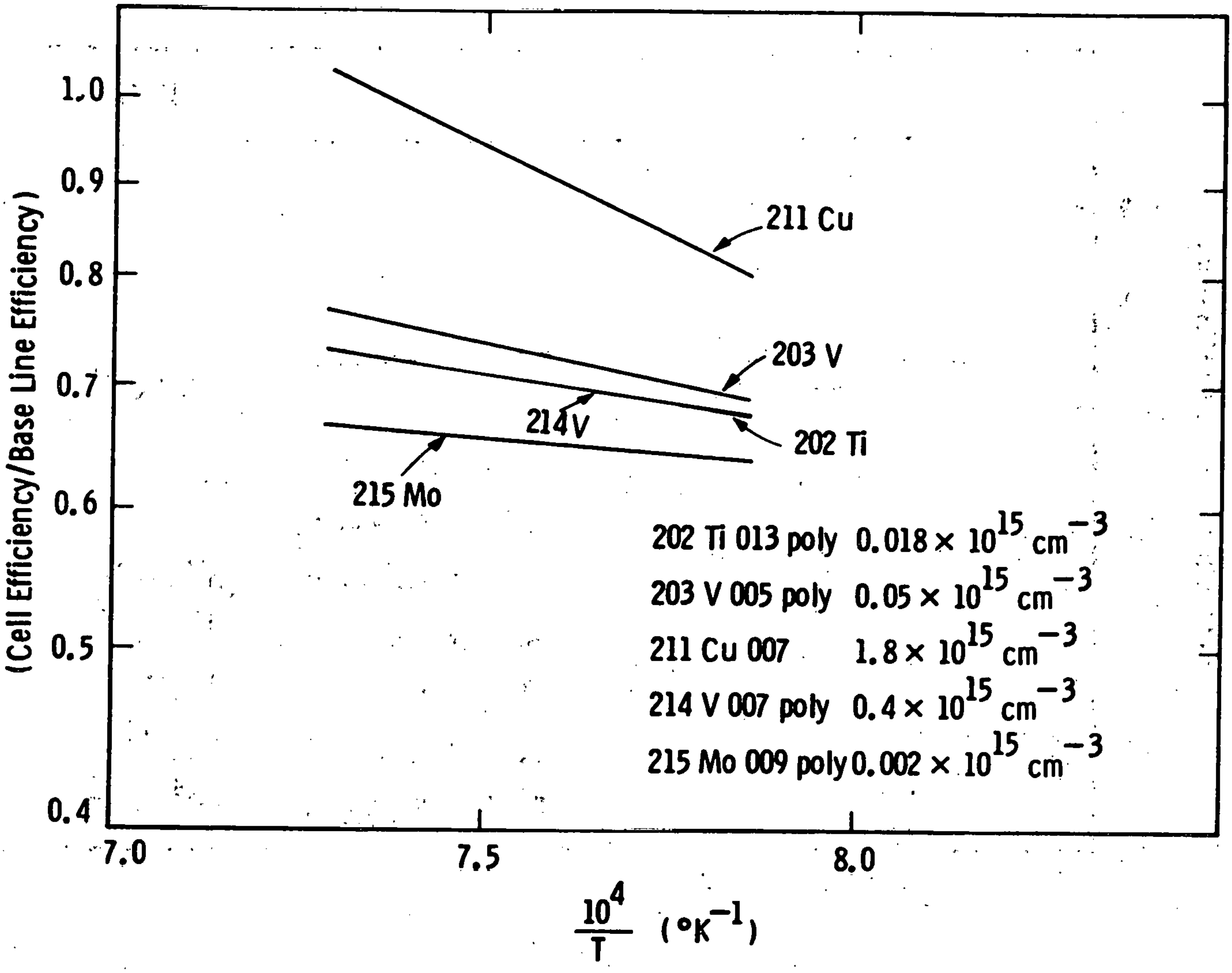

Figure 14. Gettering of Titanium, Vanadium, and Molybdenum from Polycrystalline Silicon and of Copper from Single Crystal Silicon by HCℓ Treatment at 1000 and 1100°C.

standard $POC\ell_3$ diffusion process. The significance of this experiment could be very high, relative to the cost effectiveness of ion implantation processes for less pure, but low cost, solar materials.

3.5 Impurity Behavior in High Efficiency Devices

Our investigation of solar cell impurity effects has relied on a conventional device of rather conservative design. The fabrication technology was minimally complex[1] and optimized for reliability and repeatability rather than for cell efficiency. In the following discussion we refer to these as "standard efficiency" (SE) cells as distinguished from "high efficiency" (HE) cells. SE baseline cells, ie, containing no added impurities, have an AM1 efficiency of ∿14.5% with AR coatings. An analytic model was devised to relate the performance of the SE cells to their content of added impurities.[3] The model parameter obtained to characterize the impact of each impurity is its degradation threshold (N_{OX}), above which cell performance is significantly degraded. Cells containing a specific impurity at its threshold concentration will experience a 3% loss of short-circuit current and correspondingly approximately a 7% loss in efficiency as referred to baseline devices.

The model related the normalized short-circuit current (I_n) to the concentration of impurity-x (N_x) as follows:

$$(I_{n\infty}/I_n-1)^2 = C_1(1+N_x/N_{ox}) \tag{1}$$

where C1 = 0.0121 and $I_{n\infty}$ = 1.11 are model constants slightly dependent on cell design and independent of impurity effects. The efficiency is related to the short-circuit current by the empirical expression:

$$\eta = \eta_o(0.872I_n^{1.128} + 0.128I_n^{12}) \tag{2}$$

In the model derivation it was shown that the degradation threshold can be expressed as:

$$N_{ox} = D_{nb}/(L_{no}^2 V_{th} \sigma_x A_x) \tag{3}$$

where D_{nb} is the diffusivity for electrons in the p-base, L_{no} is the effective diffusion length for electrons in the base, σ_x is the effective recombination cross-section for the traps produced by impurity x, V_{th} is the thermal velocity, and A_x is the ratio of electrically active impurity centers to those metallurgically present. Of these parameters, σ_x and A_x are direct properties of the specific impurities. L_{no} and possibly D_{nb} are indirectly affected by the type and amount of impurity.

Experimentally, the ohmic-back "standard efficiency" (SE) cells used throughout the impurity effects study exhibit values of L_{no} from ∿140 to ∿180 μm and typically have a base width of ∿275 μm. Diffusion length data are obtained from measurements of the open-circuit voltage decay, short-circuit current and from modelling analysis with results in good agreement. Diffusion lengths have also been determined from spectral quantum efficiency measurements. The results are in qualitative agreement with the other methods but yield lower absolute values by a factor of 2 to 4. This discrepancy is probably a consequence of the extremely low injection levels used in measuring spectral response since it is well known that minority carrier lifetimes increase significantly at higher injection levels. Figure 15 illustrates typical measured spectral response curves for cells of three different designs and Figure 16 shows the corresponding quantum efficiency curves. Diffusion lengths obtained from these data are: Device #1, L_{no} = 204 μm; Device #2, L_{no} = 100 μm; and Device #3, L_{no} = 315 μm. The other methods of measurement gave device #1, 400 μm; Device #2, 175 μm; and Device #3, 450 μm.

High efficiency cell performance requires that the cell or its base-width exceed the absorption length of the lowest energy photons within the absorption band of silicon. It is further necessary in order to collect the generated carriers, that the diffusion length be substantially greater than the width of the device. These requirements can be satisfied only by proper design of the cell doping profiles and contact geometry, the use of high quality silicon and careful processing to minimize introducing defects or contamination. Minimizing minority carrier recombination at the surfaces and in the bulk is also necessary.

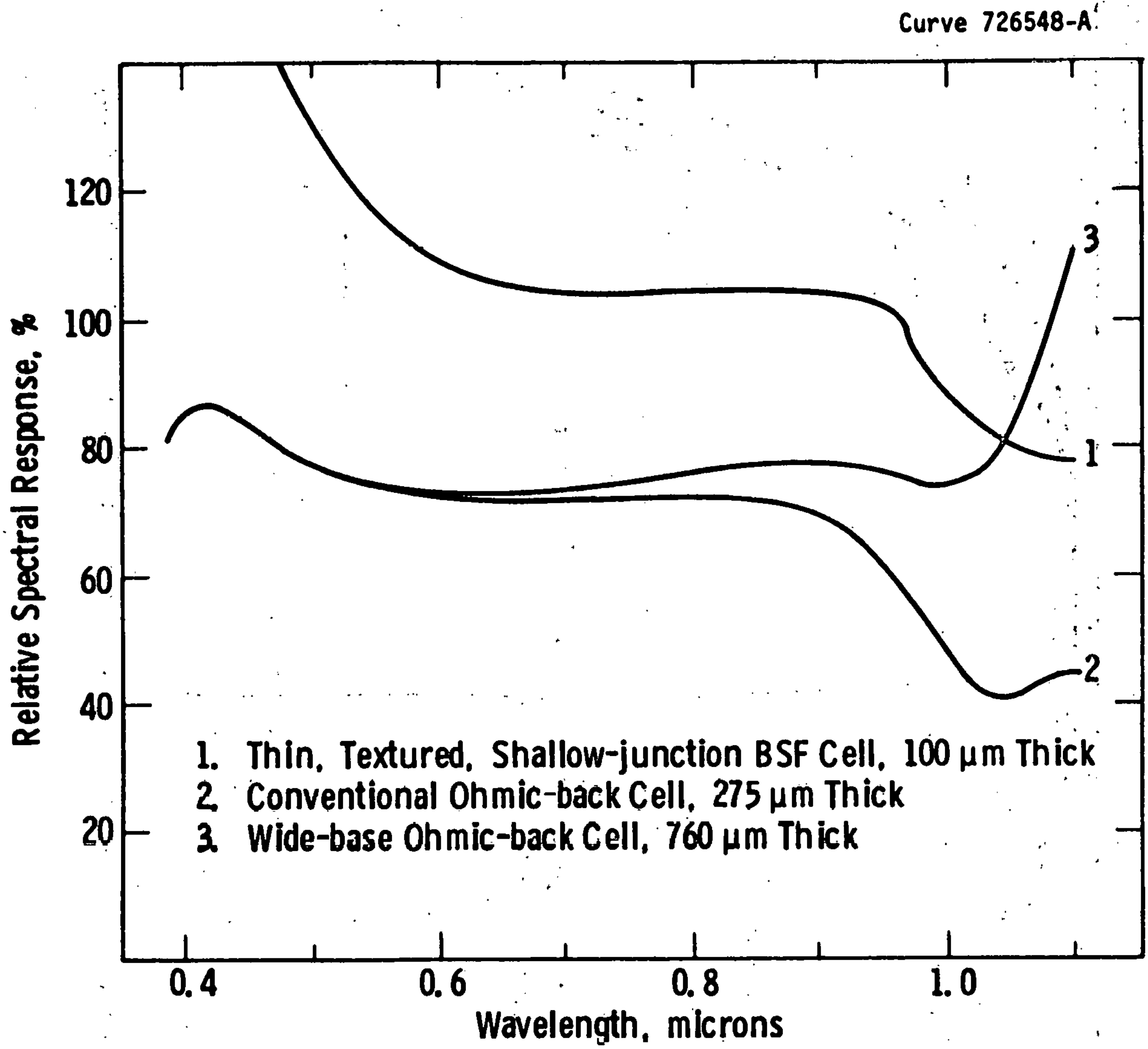

Figure 15 Measured Spectral Response for Solar Cells of Three Different Designs.

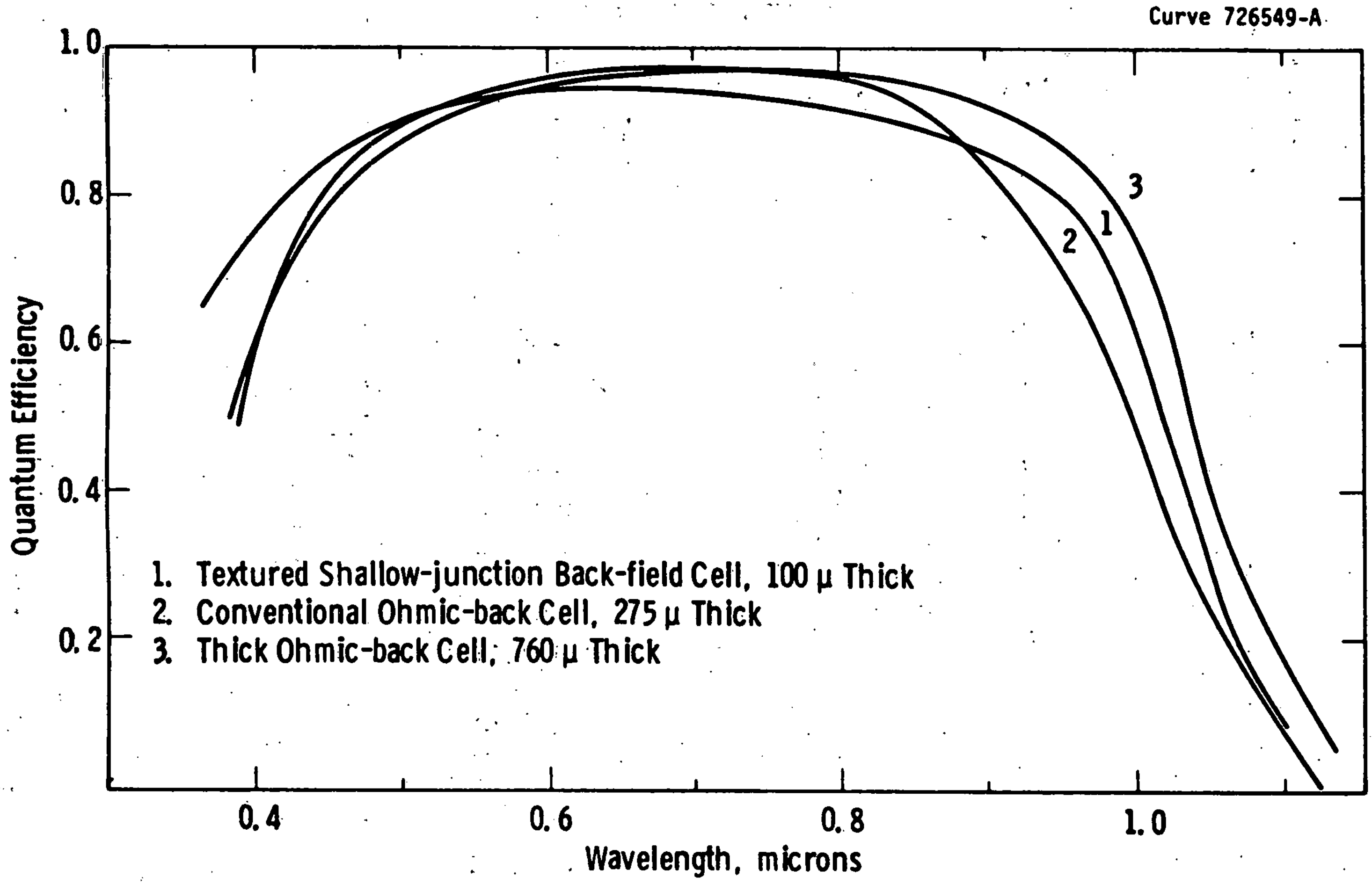

Figure 16 Quantum Efficiency Plots Corresponding to the Data of Figure 15.

Surface recombination can be reduced by the use of back-surface fields and by passivation of the physical surfaces, e.g. with oxides. Bulk recombination, although somewhat process dependent, is primarily determined by the quality of the silicon crystal; that is, its impurity content and its defect structure. The defect structure is controlled by the crystal growth technique and can be reduced to levels of little importance in crystals prepared by CZ, FZ, dendritic web and some other methods. However some casting and ribbon growth methods result in significant twinning and randomly oriented grain boundaries as well as other defects in the silicon. These defects with the exception of coherent twin boundaries have been shown to have large recombination activity even when impurities are not present. Thus for a polycrystalline material to be a likely candidate for high efficiency cells it must have very large grain structure or consist primarily of grains bounded by coherent twins.

Having identified a large effective diffusion length as a primary requirement for high efficiency, we can now examine the sensitivity of HE devices to impurities using the equations of the impurity model.[3] If we assume that the constants C_1 and $I_{n\infty}$ are independent of cell design then the model can predict the HE behavior from the data obtained with the SE devices by knowing the value of $I_{n\infty}$ required for a particular HE device. The design independence assumption is clearly questionable but as we show later, it is approximately true in the range of impurity concentrations of interest.

Using equation (3) we obtain an expression for the degradation threshold of an HE cell in terms of the value obtained for SE cells.

$$N_{ox}(HE) = N_{ox}(SE)(L_{no}(SE)/L_{no}(HE)^{2}(D_{nb}(HE)/D_{nb}(SE)) \qquad (4)$$

Let us consider the effect of adding molybdenum to a wide-base HE cell, Cell #3 in Figures 15 and 16 above. The degradation threshold for Mo in SE cells is $6 \times 10^{11}/cm^3$ and $L_{no}(SE) = 175\ \mu m$. The diffusion length in the wide-base HE cell; $L_{no}(HE) = 450\ \mu m$. These data in Equation (4) imply that the degradation threshold for Mo will be reduced to $9 \times 10^{10}/cm^3$ for the wide-base HE devices. The model curves for SE cells containing Mo are shown in Figure 17 where N_o(moly) = $6x10^{11}$. Figure 18 shows the efficiency curve for the HE device where N_o(moly) = $9x10^{10}$. By comparing the two figures it can be seen that the curve has moved to the left for the HE device indicating its approximately seven-fold higher sensitivity to the Mo concentration.

In order to test the validity of predictions of the analytic impurity model, we have developed a detailed finite element model with which we can calculate cell performance for various spectra and operating conditions. The model analysis derives from the cell design geometry and the material properties, i.e. the doping profiles, impurity content, etc. and is believed to properly include all relevant effects. Some results and a discussion of the method of analysis were presented in the previous quarterly report.

We have used this more precise model to predict the effect of molybdenum on the performance of SE cells and two types of HE cells. The results of these calculations are shown in Figures 17, 18, and 19. The agreement with the impurity model predictions and with experimental data is quite good in all three cases, at least for moderate Mo concentrations. At the highest concentrations, the impurity model predicts too great a performance loss, particularly for the narrow-base back-surface-field device, the design details of which deviate most from the assumptions used in the impurity model derivation.

For most practical purposes this analysis shows that the simple analytic expressions, Eq. (1) and Eq. (4) are suitable for determinining the impurity behavior of high efficiency solar cells. The necessary data are the values of N_{ox} for SE cells from the published data base and a value for the effective diffusion length in an uncontaminated HE cell of the required design.

Only a limited amount of experimental data is presently available for the HE cells but the results are generally in agreement with model predictions. Several experiments are in progress with both wide-base and narrow back-field devices and the results will be presented in the future.

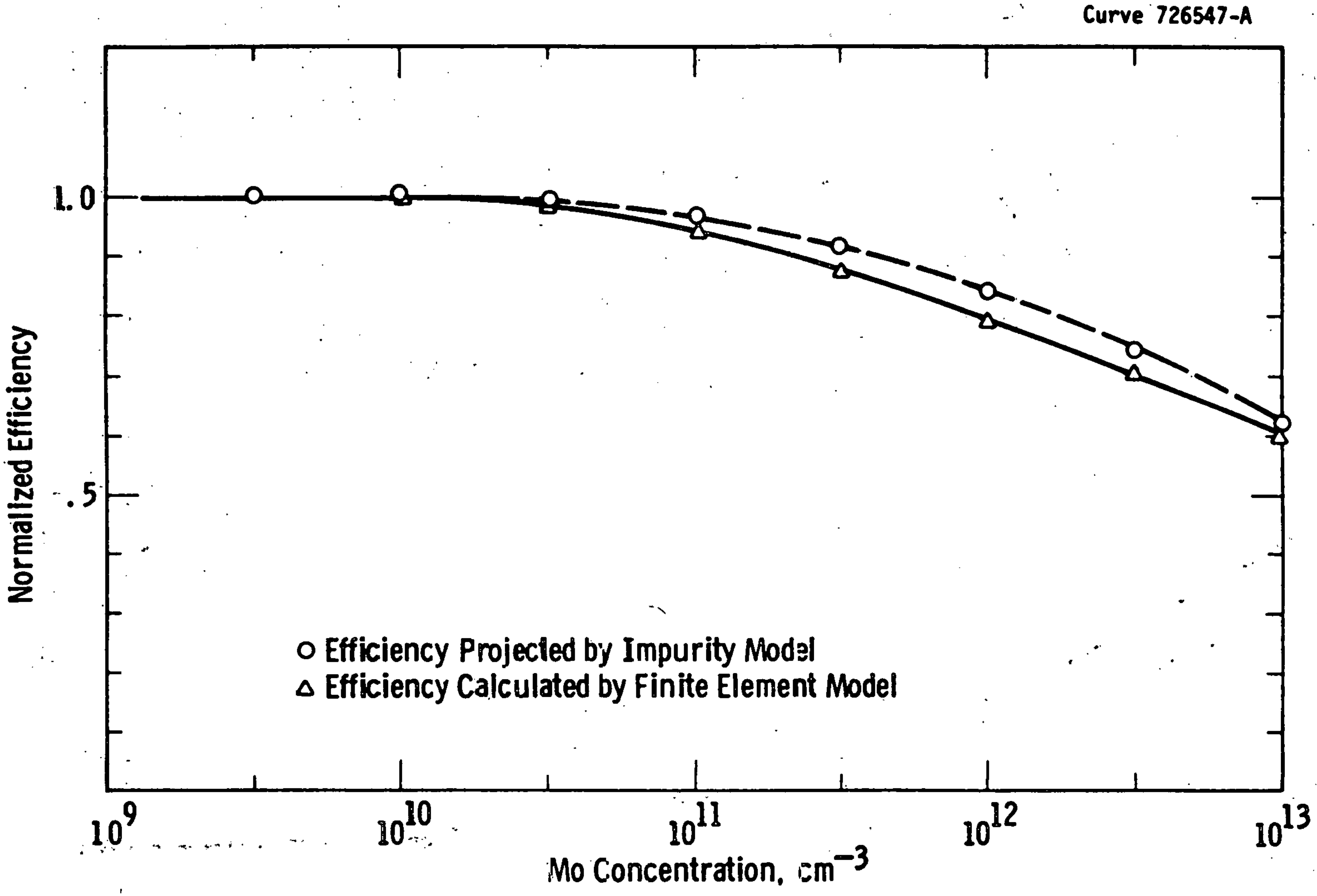

Figure 17 Calculated Cell Efficiency as a Function of Molybdenum Concentration for a Standard (SE) Design Cell ($\eta = 14\%$, $W_B = 275$ µm.)

Curve 726545-A

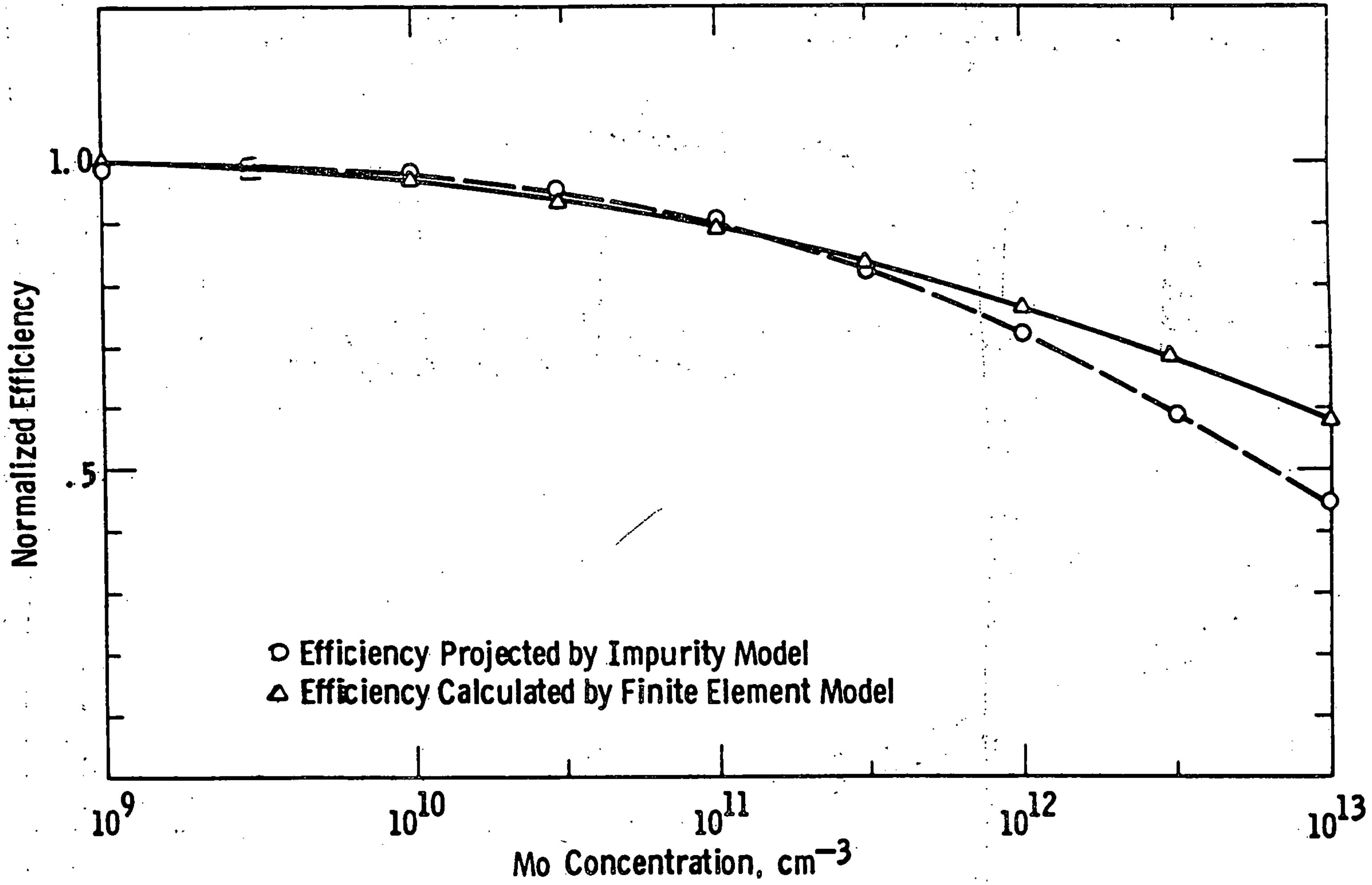

Figure 18 Calculated Efficiency as a Function of Molybdenum Concentration for a Narrow Base, Back Surface Field HE Cell (η = 15.35%, W_B = 150 μm.)

Curve 726546-A

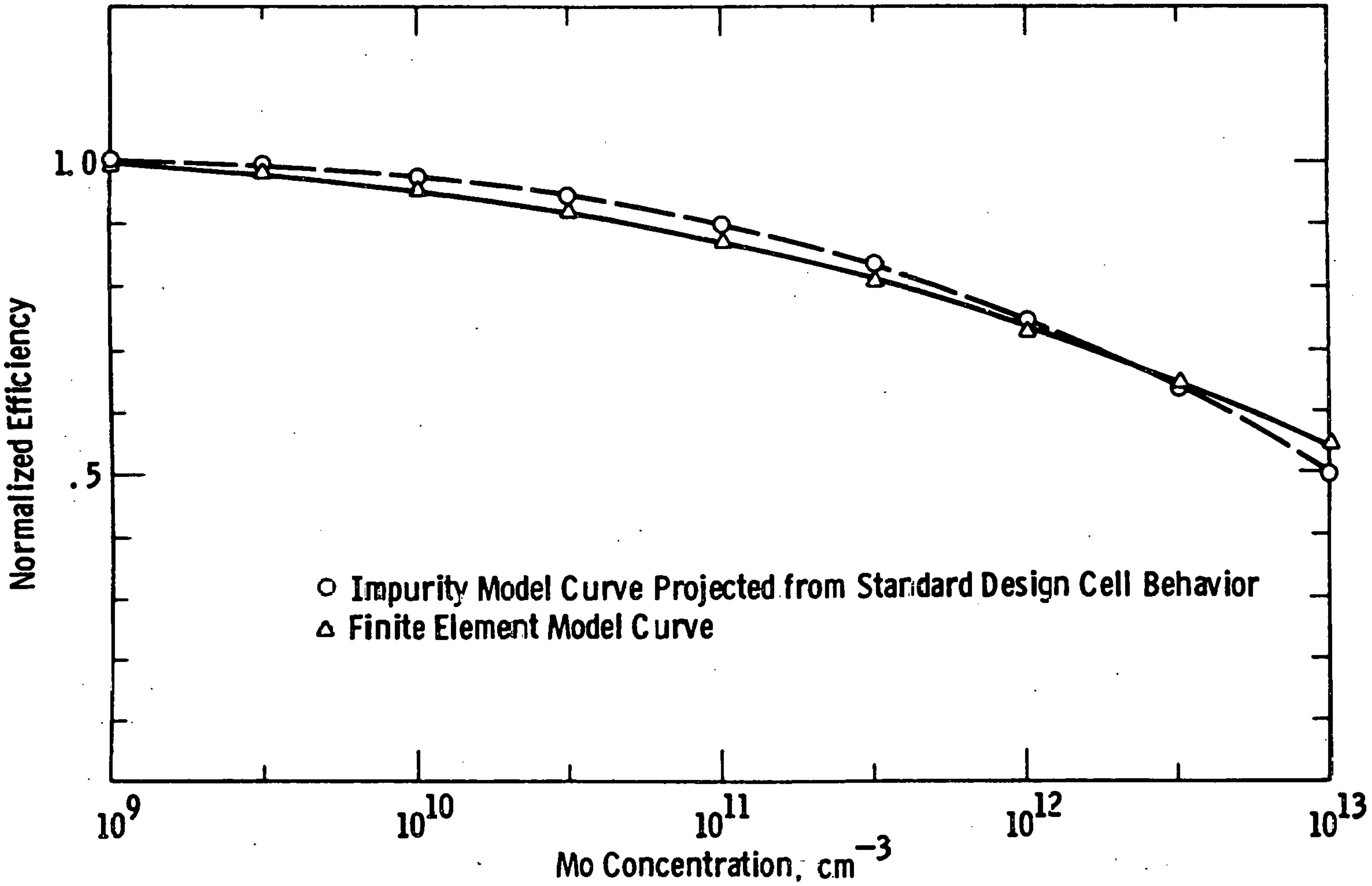

Figure 19 Calculated Efficiency as a Function of Molybdenum Concentration for a Wide Base HE Cell (η = 15.5%, W_B = 765 µm.)

4. CONCLUSIONS

Cr appears to be highly mobile in the silicon matrix even at low temperatures. We have found—in contrast to earlier results for Mo, Ti and V—that the electrically-active Cr concentrations in polycrystalline silicon vary from place to place within an ingot, and that the concentrations are more than an order of magnitude smaller than would be expected in single crystal ingots with the same metallurgical Cr content. We hypothesize the Cr diffuses to grain boundaries during cool-down from the growth temperature, becoming electrically deactivated at these locations. Spectral response data and cell performance measurements indicate cell degradation by Cr even at concentrations below the detectability by DLTS.

Even after $POC\ell_3$ gettering for only one hour at 600°C, no Cr can be detected by DLTS at depths as great as 2 mil below the surface of single crystal wafers. Prior to treatment about 8×10^{13} Cr cm^{-3} was found. Clearly rapid outdiffusion of Cr (or thermal deactivation) must occur during the treatment.

Both Aℓ and Au introduce deep levels in silicon which reduce minority carrier lifetime and cell performance. $E_V+0.44eV$ and $E_V+0.49eV$ levels are induced by Aℓ at concentrations of 1.2 and $1.7 \times 10^{12} cm^{-3}$, respectively for an ingot containing a $1.2 \times 10^{17} cm^{-3}$ metallurgical concentration. The low electrically active trap concentrations are not totally accounted for by Al-O complexing or doping effects. Au incorporated in silicon by crystal growth displays four deep levels—$E_V+0.22eV$, $E_V+0.34eV$, $E_V+0.47eV$, and $E_V+0.53eV$—in contrast to the two levels normally produced during Au diffusion. Only a fraction of the total metallurgical Au concentration is electrically active but it is sufficient to degrade bulk lifetime.

Accelerated aging of Ni-doped silicon at 400, 600, and 800°C produces a thermally-activated cell performance loss of the

$$1/\eta_o \frac{d\eta}{dt} = 28.47 \exp \left(0.673\text{eV}/kT\right)\text{hr}^{-1}$$

where η_o is the initial uncoated cell efficiency (%). Projected to a 20 year operating lifetime, the data imply no significant impact on cell performance due to Ni impurity-related effects. Data for Ag were too scattered to fit to a model of this type.

Following exposure to combined temperature and electrical bias stress for 100 hours at 225°C, solar cells containing Fe, Nb, Ag, Cr, Cu, and Ti, respectively, show no degradation in cell performance compared to baseline (un contaminated) devices. These studies will continue at higher temperatures.

Ti and V but not Mo can be gettered by either $POC\ell_3$ or $HC\ell$ treatments at 1000°C and 1100°C. This is consistent with earlier data for gettering of single crystal material containing these impurities.

Projections based on the earlier impurity-performance model and a recent, more sophisticated, finite element model show about a 7 fold reduction in the threshold for Mo content at which high efficiency cells degrade compared to our standard test device.

5. PROGRAM STATUS

The current milestone chart for the Phase IV program is illustrated in Figure 20.

5.1 Present Status

During this quarter we

- Determined the relative effects of Cr on single crystal and polycrystalline solar cells using DLTS, spectral response and cell performance data.
- Evaluated by DLTS measurements the Mo diffusion profile formed during $POC\ell_3$ gettering at 1250°C.
- Analyzed the effect of Au and Aℓ on single crystal solar cell performance.
- Completed low temperature/bias aging experiments up to 225°C on solar cells containing seven different impurities.
- Demonstrated $POC\ell_3$ gettering of Ti and V from polycrystalline solar cells.
- Correlated experimental data with model calculations for high efficiency devices.

5.2 Future Activity

During the next quarter work will continue on (1) polycrystalline cell behavior (2) thermochemical interaction of impurities, including ion implant behavior (3) permanence studies and (4) impurities in high efficiency devices.

FIGURE 20

PHASE IV PROGRAM PLAN (SCHEDULE)

TASK	J	F	M	A	M	J	J	A	S	O	N	D	J	F	M	A	M	J
	CY-1980												CY-1981					
1. Experimental Material Evaluation	▲	—	—	—	—	—	—	—	—	—	—	—	—	—	—	—	△	
2. High-Efficiency Cells	▲	—	—	—	—	—	—	—	—	—	—	—	—	—	—	—	△	
3. Polycrystalline Silicon	▲	—	—	—	—	—	—	—	—	—	—	—	—	—	—	—	△	
4. Long-Term Impurity Effects	▲	—	—	—	—	—	—	—	—	—	—	—	—	—	—	—	△	
5. Processing Studies	▲	—	—	—	—	—	—	—	—	—	—	—	—	—	—	—	△	
6. Meetings:																		
PIM	▲			▲				▲				▲				△		
Workshop											▲							
Contract Review			▲				▲			▲				△			△	
7. Reports																		
Program Plan											▲							
Monthly	▲	▲	▲		▲	▲		▲	▲		▲	▲		△	△		△	
Quarterly				▲			▲			▲			▲			△		
Final Draft																	△	
Final Report																		△
8. Deliverable Items																		
Cell Blanks																		
Cells	AS AVAILABLE																	
Silicon Materials																		

6. REFERENCES

1. R. H. Hopkins, et al., 11th Quarterly Report and Summary, Silicon Materials Task (Part 2) DOE/JPL 954331-78/3, July 1978.
2. R. H. Hopkins, et al., 5th Quarterly Report and Summary, Silicon Materials Task (Part 2) DOE/JPL 954331-77/1, January, 1977.
3. R. H. Hopkins, et al., 17th Quarterly Report and Summary-Volumes 1 and 2, Silicon Materials Task (Part 2) DOE/JPL 954331-80/9, January, 1980.
4. A. G. Milnes, Deep Impurities in Silicon, John Wiley, New York (1973).
5. K. Graff, et. al., Solid St. Elect. 16, 887, (1973).
6. R. H. Hopkins, et al., 20th Quarterly Report, Silicon Materials Task DOE/JPL-954331-80/12 October 1980.
7. J. R. Davis, A. Rohatgi, R. H. Hopkins, P. D. Blais, P. Rai-Choudhury, J. R. McCormick and H. C. Mollenkopf, IEEE Trans on Electron Devices, Vol. ED-27, No. 4, p. 677 (1980).
8. A. Rohatgi, J. R. Davis and R. H. Hopkins, IEEE Trans. on Electron Devices, Vol. ED-28, No. 1, p. 103 (1981).
9. R. H. Hopkins et al. 19th Quarterly Report, Silicon Materials Task DOE/JPL-954331-80/11, July 1980.

7. ACKNOWLEDGEMENTS

We would like to thank the following individuals whose contributions have been important to the success of this program: D. N. Schmidt (cell processing and testing), B. F. Westwood and J. McNally (process experiments and photolithography), A. M. Stewart (material characterization), H. F. Abt (metallization), S. Karako (DLTS measurements), T. Zigarovich (mask preparation), R. R. Adams and J. M. Bronner (processing), and D. Labor (manuscript preparation).

☆U.S. GOVERNMENT PRINTING OFFICE: 1981-740-145/1283